H ✓

Glaser

BRITISH JOURNAL OF

APPLIED PHYSICS

VOL. 2 NO. 10 OCTOBER 1951

Contents

THE INSTITUTE OF PHYSICS, 47 BELGRAVE SQUARE, LONDON, S.W.1

Price Six Shillings

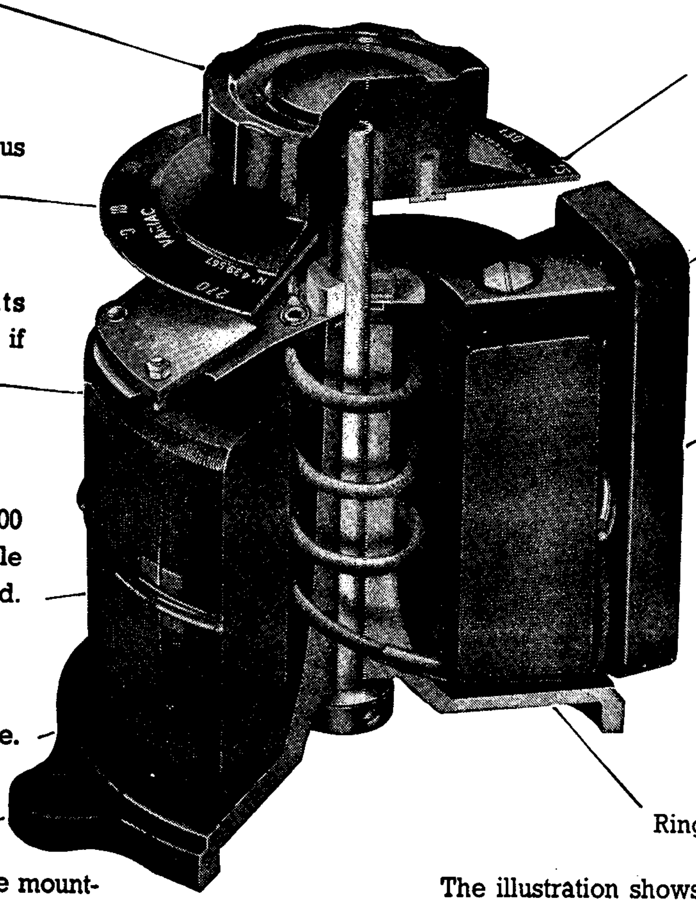

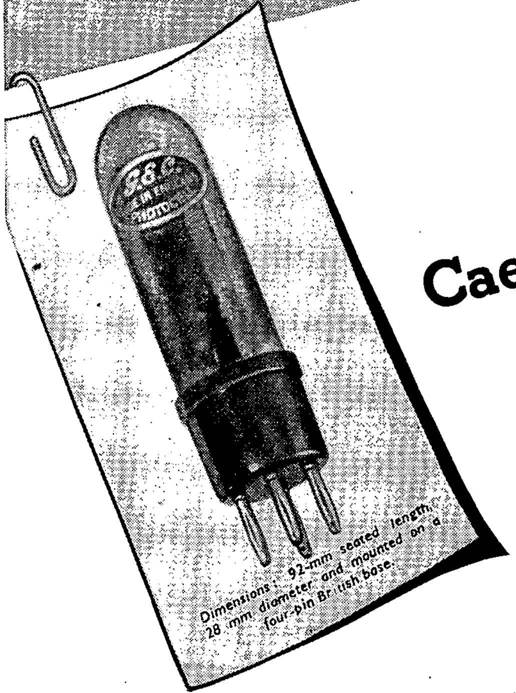

Dimensions: 92-mm seated length, 28 mm diameter and mounted on a four-pin British base.

G.E.C.

Caesium-Antimony Photocells

G.E.C. Caesium-antimony photocells, both vacuum and gas filled, are more sensitive to artificial light than caesium-silver oxide types.

The minimum sensitivity of the vacuum cell to radiation from a tungsten lamp at 2,850°K is 20μA/L, and that of the gas filled cell is 120μA/L at 90 volts with a gas factor not exceeding 8.

These cells have a peak response at the blue end of the spectrum so that for any application involving blue light, the sensitivity is vastly greater than the above figures imply.

Even though the point of highest spectral response is further from the peak of the radiant energy curve of a tungsten lamp than that of the caesium-silver oxide cell, the general sensitivity level is higher.

The caesium-antimony cell does not respond to infra-red rays but this characteristic is not without its advantages. Infra-red sensitivity is known to be closely associated with dark current which contributes to background noise in sound reproduction and similar applications.

The cathode is deposited on the wall of the bulb, so avoiding a possible source of microphony and ensuring much reduced noise level.

For further information, write to Osram Valve & Electronics Dept.

THE GENERAL ELECTRIC CO., LTD., MAGNET HOUSE, KINGSWAY, W.C.2.

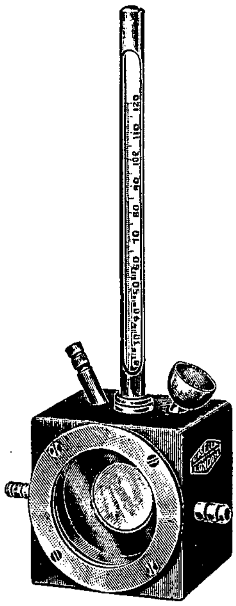

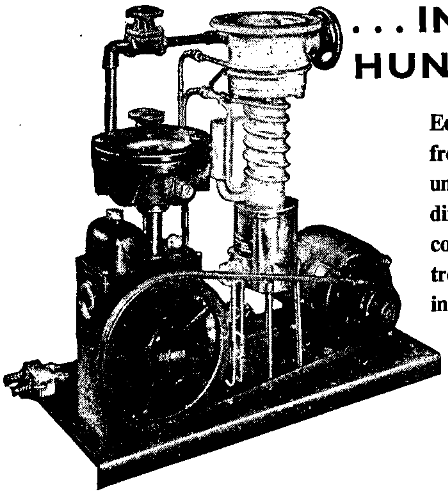

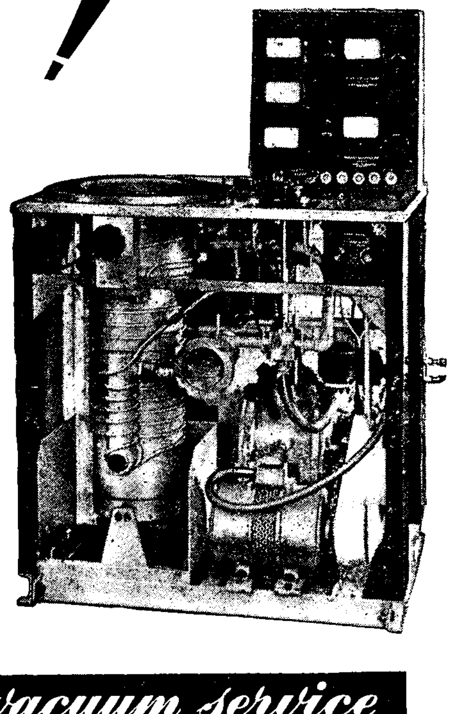

SPECIAL ARTICLE

The reinforcement of rubber by carbon black

By D. Parkinson, D.Sc., Ph.D., F.Inst.P., F.I.R.I., Research Centre, Dunlop Rubber Co. Ltd., Birmingham

Recent research on the carbon reinforcement of rubber is reviewed and existing theories examined. The stiffening effect of carbon black is thought to be little influenced by the size of the individual spherical particles, but values of tensile strength, tear strength, and abrasion resistance increase with decreasing particle size of the black. Departures from this generalization are considered and possible factors discussed. The nature of the attachments between carbon particles and rubber molecules forms the subject of much current research, the results of some of which indicate the possibility that chemical cross linkages supplement physical adsorption at the carbon-rubber interface.

Carbon black or colloidal carbon exists in a variety of forms which resemble each other in being composed of spherical or spheroidal particles, but differ from each other mainly in the size of the particles which range from 5 to 500 mμ in diameter. About 90% of the world's production of carbon black, which now amounts to upwards of 700 000 tons per annum, is used as a reinforcing agent for rubber. Reinforcement of vulcanized rubber implies increase in stiffness and tensile strength, together with resistance to tearing and abrasion. Within the range of particle sizes of the carbon blacks employed by the rubber industry the degree of reinforcement in general increases as the particle diameter decreases, the practical low limit being reached at about 20 mμ.

The remarkable wear-resisting properties of tyre treads depend primarily on the incorporation into the rubber of about one-fourth of its volume of reinforcing carbon, which until recently was all of the type known as "channel black." This substance is produced by an impingement process in which natural gas is burnt in small flames in a limited supply of air, the carbon resulting from the partial combustion being deposited on relatively cool iron "channels" which move to and fro over the flames. Rubber-grade channel blacks consist of spherical particles of average diameter 25–30 mμ.

Within recent years there has been a tendency towards the replacement of channel blacks by the so-called furnace blacks which are produced either from natural gas or from oil by incomplete combustion in large furnaces in a controlled supply of air. The resulting particles of carbon are carried along in the spent reaction gases and collected by a combination of electrostatic and centrifugal precipitation. The particle size-range for furnace black is 25–85 mμ, the fully reinforcing types averaging 30 mμ.

Other blacks that are used to a limited extent in rubber are lamp-black, formed by incomplete combustion of oils and tars, thermal black, made by thermal decomposition of natural gas and similar hydrocarbons, and acetylene black, produced by thermal decomposition of acetylene. An account of carbon black manufacture and properties by W. R. Smith(1) can be recommended as probably the most up-to-date general contribution to the subject. Earlier articles by Wiegand,(2) Cadman,(3) Cohan,(4) Drogin and Bishop,(5) and Speedy(6) contain much useful information.

The United States is the world's principal producer of the various types of carbon black. Lamp-black has long been made in the United Kingdom. A small quantity of thermal black is now being manufactured in Britain and, more important, two plants have recently started production of fully reinforcing furnace black.

Although the mechanism of carbon reinforcement of rubber is as yet very imperfectly understood, the literature on the subject is considerable and is increasing rapidly. A critical review by the author of research published up to 1944 appeared in 1946.(7) Some of the views expressed in that contribution are now in need of revision.

PROPERTIES OF CARBON BLACK

As revealed by the electron microscope, carbon black particles, with rare exceptions, are essentially spherical or spheroidal in shape. To varying degrees, according to the method of manufacture, they aline themselves into chain-like structures, the tendency to form such structures being greater for acetylene black than for other types. These chains of particles form the basis of electrically conductive rubber.

The intensity of blackness of the carbon depends primarily on particle size, the smallest particle blacks (5–20 mμ) produced by the channel process being used as pigments in the paint and ink industries. The rubber-grade channel blacks are rather greyer and coarser and the furnace and thermal blacks are coarser still in that order. Any given sample shows a size distribution of particles, and in this respect the furnace blacks are less uniform than the channel blacks. Furnace blacks, moreover, exhibit more chain structure than do channel blacks.

The mean particle diameters and specific surfaces of a

Diameter and surface area of carbon blacks

Type	*Symbol*	*Mean particle diameter, mμ*	*Surface area from size distribution, m^2/g*	*Surface area from nitrogen adsorption, m^2/g*
Medium thermal	MT	300–500	—	8
Fine thermal	FT	120–200	—	15
Semi-reinforcing furnace	SRF	80	26	22
High modulus furnace	HMF	60	38	34
Fine furnace	FF	39	59	75
High abrasion furnace	HAF	27	89	86
Medium processing channel	MPC	25	106	120
Hard processing channel	HPC	24	105	142

selection from the large number of types of carbon black used in the rubber industry are listed in the table.

Surface area determinations by low-temperature adsorption isotherms indicate that most carbon blacks are non-porous. In the case of the finest of the channel blacks the measured surface is three to four times that computed from the diameter as seen in the electron microscope, indicating in the view of W. R. Smith and others(1, 8, 9) a considerable degree of porosity.

X-ray diffraction studies have established the presence in carbon black of turbostratic(10) structure, the two-dimensional graphitic layers being parallel, but otherwise in random orientation. Heating to very high temperatures causes the crystallites to grow and to assume a more orderly arrangement, as in graphite. Carbon black treated in this way largely loses its capacity to reinforce rubber.

Chemically carbon black consists of carbon with hydrogen and oxygen varying in quantity according to the method of manufacture. The hydrogen seems to be distributed throughout the particle, but the oxygen is chemisorbed on the particle surface supposedly in the form of carbon-oxygen complexes. Furnace blacks contain less than ½% of oxygen, but in channel blacks the quantity ranges from 3 to more than 10%. The pH of the water sludge of carbon black decreases with increasing chemisorbed oxygen. Channel blacks, with a low pH value, have a retarding effect on the rate of vulcanization of rubber.

STIFFENING EFFECT OF FILLERS

The most obvious effect of the incorporation of finely divided powders or fillers in rubber is the increase in stiffness imparted to the vulcanizate. The rubber technologist defines stiffness or "modulus" as the stress at a given extension or compression. The stiffness increases progressively with increasing quantity of filler in the rubber and some of the increase is due merely to a dilution of the rubber phase by replacement with filler. Probably all the stiffening can be accounted for in this way in the case of the coarse fillers which merely act as diluents and stiffen only to a minor degree.

The stiffening effect under tension of a reinforcing material having spherical particles such as the various carbon blacks has been shown(7, 11, 12, 13, 14) to have relatively little dependence upon particle diameter, and in this respect stiffness differs from other reinforcing properties such as tensile strength and abrasion resistance which are highly dependent on particle diameter. A factor influencing stiffness is the degree of chain structure exhibited by the black when dispersed in rubber; the greater the structure the higher the modulus. To account for the major effects of stiffening it seems necessary to postulate some kind of attachment of the filler particles to the rubber molecules. The possible nature of such association is considered later.

Gehman(15) has considered the problem by regarding the filler particles as providing restraining surfaces between films of rubber. If instead of filler particles a series of parallel plates are passed through a block of rubber there will be no increase in stiffness under compression if the plates are lubricated; otherwise the plates will act as restraining surfaces and cause an apparent stiffening of the rubber. From consideration of the packing of spheres between films of rubber and of "shape factors" Gehman shows that the thickness of the rubber film between particles for a given volume concentration is proportional to the particle diameter, and deduces that if the type of packing does not change "the stiffness of the film should depend on the volume loading" (i.e. concentration) "but not on the particle size." This statement is approximately true in the case of tension stiffness. Under compression smaller particles tend to give greater stiffness than larger ones, which is explained by Gehman on the supposition that compression stiffness depends not only on shape factor but to some extent on the actual thickness of the film.

Theoretical approaches to the problem of the stiffening action of fillers have been made by Rehner(16) and Smallwood(17) from considerations of stresses in the rubber in the region of spherical filler particles. Rehner deduces that these stresses are independent of particle size and depend only on concentration of filler. Smallwood points out that because of the similarity between the field equations of the theory of elasticity and those of hydrodynamics his approach is substantially the same as that of Einstein,(18) who considered the increase in viscosity caused by suspension of spherical particles in the liquid, and the result is the same except that viscosity is replaced by Young's modulus E in Einstein's equation

$$\eta^* = \eta(1 + 2\cdot 5c) \qquad (1)$$

where η^* and η are the viscosities of the emulsion and solvent respectively and c is the volume concentration. Smallwood found therefore that the relative modulus E^*/E is directly proportional to the volume concentration and independent of the particle size of the filler.

Carefully controlled experiments were carried out by Smallwood on a series of rubber vulcanizates containing different fillers in varying proportions. Close agreement with theory was shown in the case of the thermal blacks which consist of relatively coarse spherical particles that disperse easily in rubber, but a large departure from theory in the case of the much finer channel blacks which are more difficult to disperse. The high moduli found were attributed primarily to flocculation of the black and the general conclusion was reached that the Einstein equation applies under the idealized conditions of a relatively small concentration of spherical particles, completely dispersed and with complete adhesion between the particles and the rubber matrix when the rubber is stretched to small elongations.

Guth(19) also regarded the problem as analogous to that presented by the theory of viscosity and pointed out that if a rubber-black compound is stretched the suspended particles perturb the stresses and strains, which leads to an increase in the elastic constants or, in other words, to a stiffening of the vulcanizate. Guth and Gold(20) had previously added a second term to the Einstein equation by computing the hydrodynamic interactions of pairs of particles. This equation, with Young's modulus E replacing the viscosity, may be written

$$E^* = E(1 + 2\cdot 5c + 14\cdot 1c^2) \qquad (2)$$

and Guth showed that it agreed with experiment in the case of relatively low concentrations of semi-reinforcing furnace black in GR-S synthetic rubber.

Because of the presence of chain-like aggregates as well as fully dispersed particles of carbon black in the rubber the stiffness at concentrations greater than 10% by volume increases more rapidly than is predicted from theory, and Guth, by considering rod-like particles of filler embedded in a continuous matrix, derived the expression

$$E^* = E(1 + 0\cdot 67fc + 1\cdot 62f^2c^2) \qquad (3)$$

in which f is a shape factor of the rod.

Cohan(14) in work designed to test the validity of the above equations, pointed out that although they were derived for Young's modulus they should also hold for modulus as ordinarily understood by the rubber technologist (i.e. stress at a given strain) "provided the stress-strain curves are such that the ratios of the modulus at one loading" (i.e. concentration of filler) "to that at another is the same at all elongations up to the one at which modulus is measured; that is the curves belong to a single parameter family." He found that in the case of a finely divided calcium carbonate up to a concentration of 40% by volume close agreement of the "modulus" at 300% extension with the theoretical curve of Guth and Gold. The data for a high-modulus furnace black indicated a more rapid increase in stiffness than that for calcium carbonate and the modulus-concentration curve up to 28% agreed approximately with Guth's equation for rod-shaped particles with the shape factor f equal to six. This black consists of spherical particles in which chain structure is pronounced. Cohan's results, like those of other workers and in agreement with existing theories, showed no appreciable dependence of tension stiffness on particle size.

THE INFLUENCE OF CARBON BLACKS ON SOME PHYSICAL PROPERTIES OF RUBBER

Tensile strength. There are two important differences between the stiffening action of reinforcing fillers and their effects on the strength properties of rubber. In the first place the stiffening continues up to the highest practical concentration of filler (Fig. 1) whereas the tensile strength (and also the tear strength and abrasion resistance) passes through a maximum at a moderate concentration (Figs. 2 and 3). Secondly, although the stiffness is little influenced by particle size of filler the tensile strength in general increases as the particle size decreases. In natural rubber the increase in tensile strength is of the order of 40% with a fully reinforcing black. Non-black vulcanizates of the butadiene-styrene

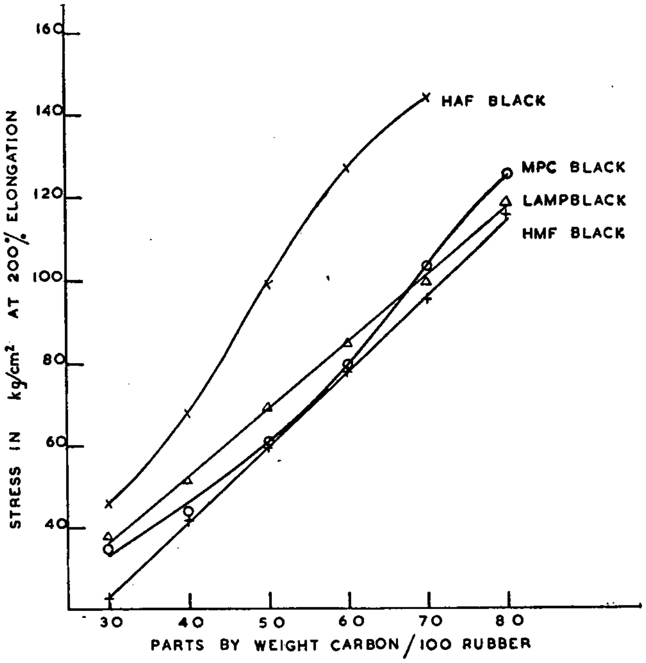

Fig. 1. Relationship between type and concentration of carbon black and stiffness of natural rubber

copolymer GR-S (the standard general-purpose synthetic rubber) have extremely low tensile strength and satisfactory physical properties are only obtainable by the incorporation of reinforcing agents. A fine particle size carbon black can, in fact, increase tensile strength of GR-S by as much as 1 000%.(13)

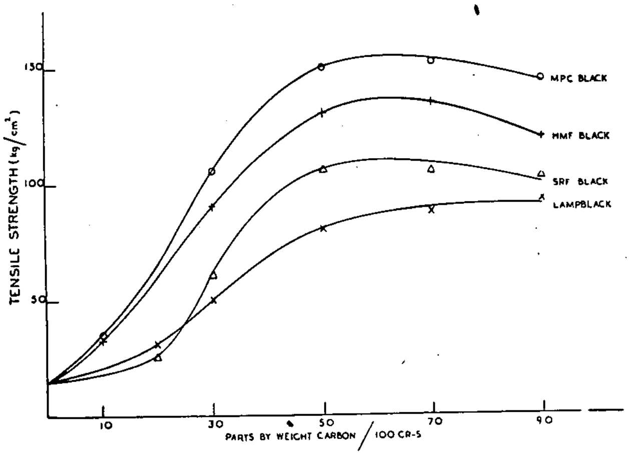

Fig. 2. Relationship between type and concentration of carbon black and tensile strength of GR-S synthetic rubber

Abrasion resistance. This property is a measure of the ability of a rubber compound to resist wear under service conditions, by far the most important instance being that of a tyre tread running on the road. Without reinforcing materials in their treads, pneumatic tyres, whether of natural or synthetic rubber, would wear out very rapidly. A four- to five-fold increase in wear-resistance of both natural rubber and GR-S is effected by the employment of a fully reinforcing black. Fig. 3 shows the relation between abrasion resistance as judged by a laboratory test specially designed to line up with tread-wear in service and the type and concentration of black added to the rubber. A general dependence of abrasion resistance upon particle diameter is indicated, but HAF black is shown to be superior to channel black although its particle size is no smaller. This point is considered later.

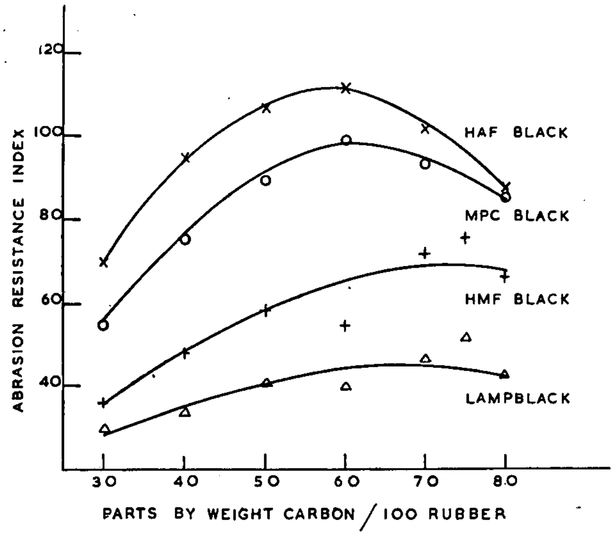

Fig. 3. Relationship between type and concentration of carbon black and abrasion resistance of natural rubber

Rebound resilience. This property progressively decreases with increased concentration of any given carbon

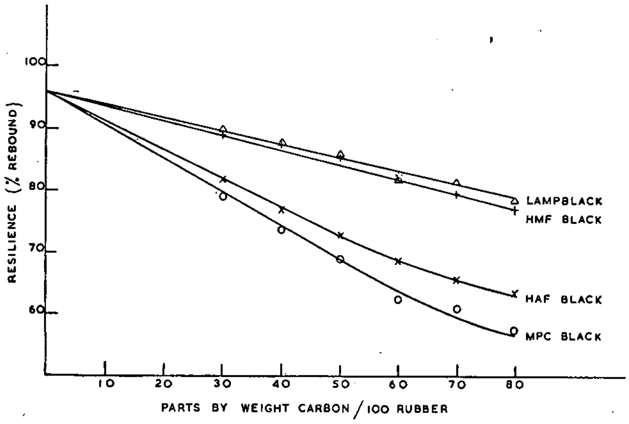

Fig. 4. Relationship between type and concentration of carbon black and resilience of natural rubber

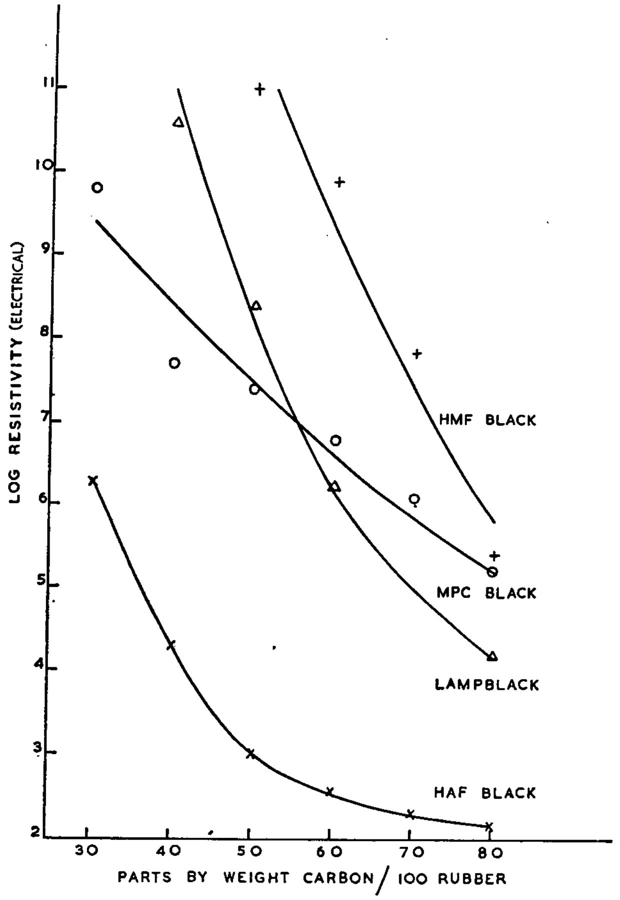

Fig. 5. Relationship between type and concentration of carbon black and specific resistance of natural rubber

black, the relationship being approximately linear up to fairly high loadings of black.(12, 13) It also decreases in general with particle diameter of black (Fig. 4), but the effect of particle size is modified somewhat according to the extent of chain structure retained by the black after incorporation in the rubber.

Electrical resistance. In Fig. 5 are plotted the changes in the logarithm of resistivity with the concentration of the same four blacks as those considered above. The curves illustrate the principle that specific resistance decreases with volume loading of all blacks and also with both particle size and chain structure of black. The requirement for an electrically conductive rubber, therefore, is a high concentration of a fine particle black which retains a high chain structure in the rubber.

ADSORPTION OF RUBBER BY CARBON BLACK

It seems necessary to postulate some kind or kinds of attachment of carbon particles to rubber molecules in order to account for the facts of reinforcement, and much recent work has had for its objective the nature of such associations which might conceivably range from physical (van der Waals) attachments to primary valence linkages.

Experiments of various kinds have been designed to show conclusively that carbon black can adsorb rubber, but in much of the work the results are capable of more than one explanation. Within recent years, however, research has thrown more light on the problem, and it is now usually conceded that adsorption of rubber by carbon black is a factor in reinforcement. The work of Goldfinger(21, 22) suggests that there is preferential adsorption of the synthetic rubber GR-S on the particles of carbon black, the fraction of the rubber left between the particles being tougher than the average of the original material. From a study of the viscosity of GR-S solutions containing channel black and the application of the Einstein viscosity equation Amborski and Goldfinger(23) inferred that under the conditions of the experiment the suspended carbon particles are surrounded by a rubber layer 150 to 200 A thick.

Work by Sweitzer, Goodrich and Burgess(24) seems to confirm Goldfinger's conclusion that carbon black selectively adsorbs the lower molecular weight fractions of rubber from dilute solution. These authors and other members of the Columbian Carbon Company(25) have developed the concept that insoluble rubber in association with carbon black or "bound rubber" is a factor in rubber reinforcement. Bound rubber or "carbon gel"(24) is formed when moderately high concentrations of finely divided carbon black are mixed into rubber, a portion of the rubber being insolubilized and held to the carbon, as has been known for many years, and can be shown when mixed unvulcanized rubber is immersed in a solvent such as benzene. The proportion of insoluble rubber increases not only with carbon concentration, but also with mixing time and temperature and time of resting before extraction. The studies of Sweitzer and others indicate that under their conditions of experimentation less than one-tenth of the insolubilized rubber is actually adsorbed on the carbon black surface and these authors postulate a "three dimensional lattice structure with carbon-rubber units joined together by additional rubber through primary and/or secondary valence forces." They also give evidence suggesting that small amounts of oxygen help to promote the development of "carbon gel." Finally they suggest that tyre tread-wear performance is improved by processing techniques which have the effect of increasing the bound rubber in the vulcanizate.

It would appear that if the insolubilization of rubber by carbon blacks is promoted under similar processing conditions it is a function of particle size. This was first suggested by Fielding in 1937(26) and has received support from work by Dannenberg and Collyer,(8) whose data show a linear relationship between bound rubber values and surface areas as measured by the electron microscope. This suggests, according to the authors, that the rubber molecules can be almost totally adsorbed on the surfaces of the carbon particles. It should be pointed out that Dannenberg and Collyer's results were obtained in rubber mixed under different conditions—e.g. at much lower temperatures—than those employed by Sweitzer and others and the bound rubber values are consequently much lower. The data of Sperberg and colleagues(27) indicate a linear relationship between bound rubber and abrasion resistance. Recent work by Stearns and Johnson(28) has led them to suggest that bound rubber is due to covalent bonding between the black and the polymer in solution.

On the whole it seems that the phenomenon of insolubilization of rubber by carbon black supports the view that molecules of rubber are adsorbed on the carbon surface but that other forces of a stronger nature than van der Waals attachments are also involved.

HEATS OF ADSORPTION STUDIES

It is inferred that reinforcement by small spherical particles is concerned in some way with extent of the carbon-rubber interface since surface area is inversely proportional to particle diameter for a given volume of filler. The question arises as to whether reinforcement is also a function of the nature or activity of the carbon surface.

The nature of the surface of carbon particles depends upon the method of manufacture. Thus furnace blacks, which contain little volatile matter, apparently have particle surfaces consisting mainly of carbon atoms, whereas channel blacks have a chemisorbed layer consisting largely of oxygen in various kinds of combination with carbon, but some nitrogen and hydrogen are also present.(29) This difference influences the value of pH and hence the rate of vulcanization of the rubber incorporating the different blacks, the channel blacks promoting the slowest rates of vulcanization. The difference in the nature of the surface may also have an influence on reinforcing ability since furnace blacks for equivalent particle size reinforce a little more than channel blacks. A further point of interest is the fact that channel black, on partial graphitization at 3 000° C *in vacuo*, largely loses its capacity to reinforce without a significant change in the extent of surface.

In order to throw more light on the activity of carbon black surfaces and their bearing on rubber reinforcement, W. R. Smith of the Cabot Carbon laboratories and co-workers(9, 29, 30, 31, 32) have studied the heats of adsorption of various types of carbon black for a number of substances, comprising elementary gases and a series of saturated and unsaturated hydrocarbons, including dihydromyrcene, which is the simplest diolefin possessing the same unsaturation pattern as that of natural rubber. It was thought that such measurements would reflect the magnitude of the binding forces operative at carbon black surfaces and might also reveal their nature. In the case of nitrogen, oxygen and argon, and the lower molecular weight unsaturated hydrocarbons the adsorption was shown to be entirely of the van der Waals type, but with dihydromyrcene it was found that something other than physical adsorption is involved and it was suggested(9) that "the nature of association between rubber and carbon may involve the unsaturation of the elastomer and the volatile matter normally present on the carbon black." They further suggest the possibility that "a few points of exceptionally strong cross-linkage may play an important role in reinforcement, and that the small fractions of the carbon surface involved may be highly specific." The present author had previously put forward the view that in order to account for certain of the facts of reinforcement a limited number of strong bonds might be operative at the rubber-carbon interface.(7, 13)

From a study of the thermodynamical changes accompanying the deformation of reinforced rubber Stearns and Johnson(28) conclude that physical adsorption of the van der Waals type is inadequate to account for the experimental results. They endeavour to show by a calorimetric method that the surface of a carbon black particle contains sites that react with bromine to liberate the same amount of heat as low molecular weight olefins and suggest that the rubber and black are combined chemically through carbon-rubber-sulphur bonds into a continuous three-dimensional cross-linked matrix.

MOBILITY OF CARBON PARTICLES IN RUBBER

The extent to which carbon black particles can migrate in rubber has been and is still a subject of much discussion.(7, 33, 34, 35) Flocculation of particles has been invoked to explain some of the changes, and particularly changes in electrical resistance, that take place in both vulcanized and unvulcanized rubber-black compounds following different treatments. As a result of considerable research the author and Blanchard(35) reached the conclusion that although there is limited mobility of carbon particles in rubber there is no convincing evidence of extensive flocculation of discrete carbon particles into groups or a "catenation" into chains within the rubber itself. The chains of particles that undoubtedly do exist in carbon-reinforced rubber are interpreted as portions of original structures which have survived the stresses set up in the rubber during the mixing operation, though it is admitted that there is some increase in chain structure when the rubber is heated. Remilling the rubber following heat treatment under certain conditions can break down the structure permanently as is shown by the enormous increase in electrical resistivity which does not change on further heating.

Mullins and Whorlow have recently(36) discussed the changes that take place in masticated unvulcanized rubber containing fillers. Before vulcanization the rubber is in a plastic condition and it softens on shearing and stiffens on standing. Such thixotropic behaviour is small unless the rubber contains reinforcing fillers, when it is much more pronounced. Mullins and Whorlow argue that the changes can be explained by a breaking down and building up of structure and that at least two processes are involved: "(1) the orientation and/or disentanglement of both the long molecular chains" (of rubber) "and anisotropic filler particles or chains of filler particles; (2) breaking down of interactions either between neighbouring filler particles or between the filler and the rubber, or both." These authors consider that the bonds will have a range of strengths, the weak bonds breaking more readily. On standing after shearing the structures are supposed to re-form at rates depending on the temperature.

EFFECT OF STRESSING ON STIFFNESS OF CARBON-REINFORCED RUBBER

The normal tensile stress-strain test for rubber involves only the first extension, though it is well known that the shape of the stress-strain curve changes with successive deformations. This change is small for pure vulcanized rubber, but in the case of vulcanizates containing substantial concentrations of reinforcing fillers it is considerable, the greatest effect being caused by the first extension; after about six stretch-cycles a more or less steady state is reached.

The changes under consideration have been studied in detail by Mullins,(37, 38) who showed that a large part of the increased stiffness imparted to natural rubber by reinforcing agents is destroyed by stretching. The degree of softening is greater the greater the stretch and the greater the stiffening effect of the filler. Mullins found that on stretching the test-pieces after the first extension substantially all the softening occurred at elongations less than the previous extension and that at elongations in excess of the previous extension the rubber behaved as though it had not previously been stretched.

Hence the tensile strength is uninfluenced by previous stressing. Mullins considers that the softening results mainly from a "breakdown of filler structure."

Blanchard and the author$^{(39)}$ have argued that except perhaps at small stresses the stiffening bonds which are broken during stressing are largely carbon-rubber bonds and give reasons for the view that a substantial part of carbon chain structure survives no matter how severely the rubber has been stressed. Their work is consistent with the view that most of the carbon-rubber bonds are of low energy (van der Waals) type, but that a small number of strong bonds stiffen the rubber substantially at high stresses and are largely responsible for increasing the tensile strength.

Recent work by Waring$^{(40)}$ relates to the changes taking place in reinforced rubber resulting from high-frequency compression at amplitudes of the order of 0·05% of the length of the test-piece in the temperature-range of 30 to 70° C. Waring found a decrease in dynamic stiffness with increasing temperature and a decrease in electrical resistance with increasing temperature when no vibration was present, but that the application of mechanical vibration increased the resistivity. He postulates the existence of "two states of the carbon black structure," one of which has a higher and the other a lower conductivity, and visualizes vibration as promoting a thixotropic change from one to the other by producing a decatenation of the carbon structure. Temperature is supposed to have a mixed effect, on the one hand catenation of carbon particles "and at the same time a breakdown of the cohesive bonds between carbon and rubber which do not affect the conductivity but contribute a considerable effect to dynamic modulus."

COMPARISON OF FURNACE AND CHANNEL BLACKS IN RUBBER

It is now generally recognized that the finer of the furnace blacks are at least equal to channel black, both in natural and synthetic rubber.$^{(8, 27, 41, 42)}$ In their influence on abrasion resistance the high abrasion furnace blacks are even better than the rubber-grade channel blacks, but they have some disadvantages in that they are not quite so easily processed in the rubber factory.

In view of the increasing tendency of the high-abrasion furnace blacks to replace the channel blacks in tyre-tread and similar compounds, research and development work involving comparisons of the two types of black is of paramount importance at the present time. In this country the matter is of particular interest because furnace blacks made in Great Britain are beginning to replace imported channel blacks. Some recent work on this aspect of the problem is briefly considered below.

Comparisons have been made above of natural rubber vulcanizates incorporating four types of carbon black including the two types now under consideration, namely medium processing channel (MPC) and high abrasion furnace (HAF). Among the features to be noted are the higher "modulus" of the furnace-black compound due presumably to a greater development of chain structure in the HAF than in the MPC black and also its higher abrasion resistance. The question arises whether the difference in abrasion resistance is also a consequence of a difference in structure. Abrasion resistance, as we have seen, is, unlike stiffness, primarily a function of particle size. The table shows that the specific surface of HAF black is less than that of MPC black; and electron micrographs indicate that the former has a wider size distribution and greater proportion of larger particles than the latter. It is evident that the furnace black gives a higher abrasion resistance than is accounted for by its particle size and it is tempting to attribute this to an increased chain structure. However, breaking down the structure by severe remilling does not decrease abrasion resistance,$^{(43)}$ and it seems to be true that the acetylene black, with the greatest chain structure of all, imparts poor abrasion resistance in relation to particle size.$^{(7, 12)}$ Chain structure, therefore, does not in itself seem to be a major factor in abrasion resistance and the beneficial effect of furnace black may depend, as suggested earlier in this review, on a difference in the nature of the surface. Furnace blacks differ from channel blacks in having relatively little chemisorbed oxygen on the surface of the particles. The surface oxygen is largely responsible for the retarding effect of channel blacks on the rate of vulcanization and it is possible that it influences physical properties. Dannenberg and Collyer$^{(8)}$ have shown that the results of calcining channel black to remove the surface oxygen are an increase in the rate of vulcanization and an improved laboratory abrasion resistance by about 10%. They conclude that calcined MPC black is about equal to HAF black in laboratory abrasion resistance and suggest that "a factor responsible for high abrasion furnace black superiority over a channel black of equivalent particle size is its relative freedom from chemisorbed surface oxygen." Dannenberg and Collyer also considered "bound rubber" as a possible factor, but since under their conditions of experimentation bound rubber was found to be linearly related to surface area it did not help to explain the increased capacity of HAF blacks over channel blacks to reinforce rubber.

CONCLUSIONS

It will be evident from the foregoing considerations that existing theories of rubber reinforcement are incomplete and that many of the facts await a satisfactory explanation. For a fuller understanding of the mechanism of the process it is necessary to determine the nature of the association between carbon particles and rubber molecules. It is generally agreed that van der Waals forces, which are of low energy, are operative, but these do not account for all the experimental observations. Recent work of various kinds$^{(9, 24, 28, 39)}$ indicates the possibility that chemical cross-linkages may play an important part in the carbon reinforcement of rubber. Here, then, are opportunities for research in which the special methods developed by physicists can be of the greatest value to industry.

REFERENCES

(1) Smith, W. R. *Encyclopedia of Chemical Technology*, **3**, p. 34 (New York: Interscience Encyclopedia Inc., 1949).

(2) Wiegand, W. B. *Can. Chem. and Proc. Ind.*, **28**, p. 151 (1944).

(3) Cadman, W. H. *J. Roy. Soc. Arts*, **94**, p. 646 (1946).

(4) Cohan, L. H. *Chem. Engng. News*, **23**, p. 2078 (1945).

(5) Drogin, I., and Bishop, H. R. *To-day's Fuenace Blacks* (Charleston: Charleston Printing Co., West Virginia, 1947).

(6) Speedy, A. *Soc. Chem. Ind.*, No. 39, p. 354 (1946).

(7) Parkinson, D. *Advances in Colloid Science*, **2**, p. 389 (New York: Interscience Publishers Inc., 1946).

(8) Dannenberg, E. M., and Collyer, H. J. *Industr. Engng. Chem.*, **41**, p. 1607 (1949)

(9) Schaeffer, W. D., Polley, M. H., and Smith, W. R. *J. Phys. Coll. Chem.*, **54**, p. 227 (1950).

(10) Biscoe, J., and Warren, B. E. *J. Appl. Phys.*, **13**, p. 364 (1942).

(11) Wiegand, W. B., and Ladd, W. A. *Rubber Age* (New York), **50**, p. 431 (1942).

(12) Parkinson, D. *Trans. Instn. Rubb. Ind.*, **19**, p. 131 (1943).

(13) Parkinson, D. *Trans. Instn. Rubb. Ind.*, **21**, p. 7 (1945).

(14) Cohan, L. H. *India Rubber World*, **117**, p. 343 (1947).

(15) Gehman, S. D. *Industr. Engng. Chem.*, **36**, p. 715 (1944).

(16) Rehner, J. *J. Appl. Phys.*, **14**, p. 638 (1943).

(17) Smallwood, H. M. *J. Appl. Phys.*, **15**, p. 758 (1944).

(18) Einstein, A. *Ann. Phys., Paris*, **19**, p. 289 (1906); **34**, p. 591 (1911).

(19) Guth, E. *J. Appl. Phys.*, **16**, p. 20 (1945).

(20) Guth, E., and Gold, O. *Phys. Rev.*, **53**, p. 322 (1938).

(21) Goldfinger, G. *Rubber Chem. Tech.*, **18**, p. 286 (1945).

(22) Goldfinger, G. *J. Polymer Res.*, **1**, p. 58 (1946).

(23) Amborski, L. E., and Goldfinger, G. *Rec. Trav. Chim. Pays-Bas*, **68**, p. 733 (1949).

(24) Sweitzer, C. W., Goodrich, W. C., and Burgess, K. A. *Rubber Age* (New York), **65**, p. 651 (1950).

(25) Braendle, H. A., Estelow, R. K., and Weigand, W. B. *Rubber Age* (New York), **67**, p. 64 (1950).

(26) Fielding, J. H. *Industr. Engng. Chem.*, **29**, p. 280 (1937).

(27) Sperberg, L. R., Svetlik, J. F., and Bliss, L. A. *Industr. Engng. Chem.*, **41**, p. 1641 (1949).

(28) Stearns, R. S., and Johnson, B. L. *Industr. Engng. Chem.*, **43**, p. 146 (1951).

(29) Smith, W. R., and Schaeffer, W. D. *Proceedings of the Second Rubber Technology Conference*, p. 403 (Cambridge: W. Heffer and Sons Ltd., 1948).

(30) Beebe, R. A., Biscoe, J., Smith, W. R., and Wendell, C. B. *J. Amer. Chem. Soc.*, **69**, p. 95 (1947).

(31) Beebe, R. A., Polley, M. H., Smith, W. R., and Wendell, C. B. *J. Amer. Chem. Soc.*, **69**, p. 2294 (1947).

(32) Beebe, R. A., Kington, G. L., Polley, M. H., and Smith, W. R. *J. Amer. Chem. Soc.*, **72**, p. 40 (1950).

(33) Bulgin, D. *Trans. Instn. Rubb. Ind.*, **21**, p. 188 (1946).

(34) Wack, P. E., Anthony, R. L., and Guth, E. *J. Appl. Phys.*, **18**, p. 456 (1947).

(35) Parkinson, D., and Blanchard, A. F. *Trans. Instn. Rubb. Ind.*, **23**, p. 259 (1948).

(36) Mullins, L., and Whorlow, R. W. *Trans. Instn. Rubb. Ind.*, **27**, p. 55 (1951).

(37) Mullins, L. *J. Rubber Res.*, **16**, p. 275 (1947).

(38) Mullins, L. *J. Phys. Coll. Chem.*, **54**, p. 239 (1950).

(39) Blanchard, A. F., and Parkinson, D. *Proceedings of the Second Rubber Technology Conference*, p. 414 (Cambridge: W. Heffer and Sons Ltd., 1948).

(40) Waring, J. R. S. *Industr. Engng. Chem.*, **43**, p. 352 (1951).

(41) Sperberg, L. R., and Barton, H. M. *Rubber Age* (New York), **63**, p. 45 (1948).

(42) Parkinson, D. *Trans. Instn. Rubb. Ind.*, **24**, p. 267 (1949).

(43) Parkinson, D. *Trans. Instn. Rubb. Ind.*, **16**, p. 88. (1940).

ORIGINAL CONTRIBUTIONS

Aerial prospecting for radioactive minerals

By D. H. Peirson, B.Sc., A.Inst.P., and E. Franklin, Ph.D., Atomic Energy Research Establishment, Harwell, Berks

[*Paper first received* 2 *January*, 1951, *and in final form* 2 *May*, 1951]

The γ-ray flux over a radioactive mineral deposit has been calculated and expressions derived for the variation with operational flying conditions. An airborne equipment comprising 49 Geiger-Müller tubes was designed to investigate the overall sensitivity and the practical problems arising from the use of such a method of prospecting. Thus a surface mineral deposit of concentration factor (% U_3O_8 by weight) × area (sq yd) of about 100 is just detectable above "background" fluctuations at an altitude of 500 ft overhead and speed of 120 m.p.h. The effect of deposit and background activity upon the comparative performance of Geiger and scintillation counters is such that a practical improvement of three times may be expected from the scintillation counter.

1. INTRODUCTION

The possibility of conducting a survey of radioactivity by air over areas of virgin country has attracted the interest of geologists. Not only does such a method of survey increase the convenience of a systematic search, but the speed of covering a given area, possibly barely accessible on foot, is greatly increased. The use of aircraft for similar purposes has been successfully demonstrated in magnetometer and photographic surveys. Provided that an accurate means of navigation is available, the area may be traversed according to a simple flight plan and with the assurance that all obtrusive radioactive deposits above a certain minimum strength, dependent upon the sensitivity of the detecting apparatus, will be located. A deposit discovered in this manner can be referred to a ground party for fuller investigation. In aerial prospecting the sensitivity and response of the detecting apparatus are in part dependent upon the altitude and speed of flight, and hence upon the choice or availability, of different aircraft. For a given sensitivity, a lower limit to detection will be set by the fluctuations in response to background activity. The background effect arises from cosmic rays and from local natural radioactivity. The local component is due mainly to the active content of the earth's surface (generally equivalent to about 0·001% concentration of U_3O_8) together with possible effects due to atmospheric activity, and to active contamination of the walls of equipment and aircraft. A variation of background with altitude may be expected. In order to establish the optimum conditions of design and adjustment in the detecting apparatus, it is desirable to calculate, with reasonable accuracy, the inter-dependence of the several operational variables, i.e. the relations between sensitivity and speed of response ("time constant") and altitude, distance and aircraft speed.

There are three methods of detection suitable for aerial prospecting. These are based on the use, with appropriate circuits and recorders, of (i) ionization chambers, (ii) Geiger counters, and (iii) scintillation counters. Geiger counters were adopted for this present work because of their greater discrimination against cosmic background as compared with ionization chambers. Potentially, the scintillation counter provides greater advantages than the Geiger counter but the technique was considered insufficiently developed to permit reliable and consistent operation in an airborne equipment.

2. γ-RAY FLUX AND DETECTOR RESPONSE

2.1. *Statement of problem.*—It is required to calculate the γ-ray flux at any altitude and range due to a deposit of given surface area. An ideal flat earth's surface is assumed. The expression for γ-ray flux is determined by an inverse square factor together with exponential decay terms due to absorption within the deposit and absorption in the atmosphere. The flux expression, integrated over the whole deposit, is introduced in the differential equation controlling the time response of the detecting apparatus. The peak detector signal is then derived as a function of altitude, speed, range, background deviation and other factors.

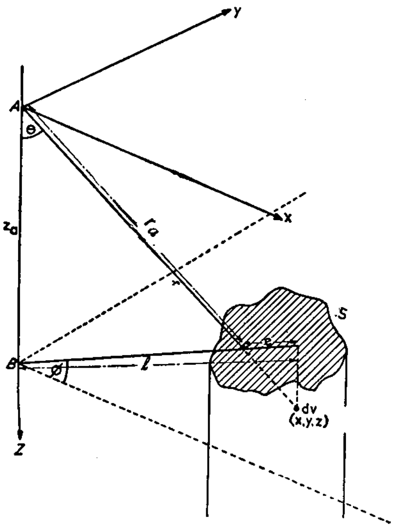

Fig. 1. Geometry of aircraft and deposit

2.2. *γ-ray flux.*—With reference to Fig. 1, consider a detector of area *A* situated at the origin of the coordinates and a radioactive mineral "deposit" of infinite depth with surface S at ground-level in the z_a plane. The solid angle subtended by A at an elementary volume dV situated at x, y, z within the deposit

$$= \frac{A}{r^2} \text{ where } r^2 = x^2 + y^2 + z^2$$
$$= l^2 + z^2$$

Then, taking account of absorption within the deposit and absorption in the atmosphere, the γ-flux (dI) from dV incident upon A is given by

$$dI = \frac{A}{4\pi r^2} \cdot N\rho_s dV \,.\, \epsilon^{-\mu_s(r-r_a)}\,\epsilon^{-\mu_a r_a}$$

where $N = \gamma$ activity of deposit/unit mass/unit time.
$r_a =$ distance in air between A and dV.
$\rho_s =$ density of the deposit and also of the surrounding earth.
$\mu_s = \gamma$ absorption coefficient of the deposit, and also of the surrounding earth.
$\mu_a = \gamma$ absorption coefficient of air.

μ_s and μ_a represent values of the absorption coefficients weighted according to the intensity and energy distribution of the γ-radiation. Values for μ_a have been tabulated by Heitler:(1) the value chosen in the following computations is $\mu_a = 0{\cdot}0001 \text{ cm}^{-1}$. This may be in error by 30%.

Assuming A has spherical symmetry, the total γ-flux through A due to the whole deposit

$$I = \frac{NA\rho_s}{4\pi}\int_V \frac{1}{r^2}\,\epsilon^{-\mu_s(r-r_a)}\epsilon^{-\mu_a r_a}dV$$

This integration is carried out in Appendix 1: it is shown that, to a close approximation,

$$I = \frac{NA\rho_s}{4\pi}\cdot\frac{1}{\mu_s z_a}\int_S \frac{\epsilon^{-\mu_a\sqrt{(l^2+z_a^2)}}}{(l^2+z_a^2)^{\frac{1}{2}}}dS \qquad (1)$$

where l, equal to $\sqrt{(x^2+y^2)}$, represents the range of A from the elementary surface area dS.

Provided that the linear dimensions of S are small compared with the altitude z_a, the quantity l and hence the integral, dependent upon $(l^2 + z_a^2)^{\frac{1}{2}}$, will vary little over the extent of S. It is possible to select a mean range $\bar{l}$ for the whole surface area such that, with good accuracy,

$$I = \frac{NA\rho_s}{4\pi}\cdot\frac{S}{\mu_s}\cdot\frac{\epsilon^{-\mu_a\sqrt{(\bar{l}^2+z_a^2)}}}{z_a(\bar{l}^{-2}+z_a^2)^{\frac{1}{2}}} \qquad (2)$$

Strictly (2) refers only to a point deposit. The errors introduced by applying it to a finite area have been determined by comparison with the numerical computation of the integral (1), showing that, for a circular deposit area of diameter $z_a/5$ the error is within 1% over the range $\bar{l}/z_a = 0$ to 3. For the particular (and simpler) case where the aircraft is immediately overhead (i.e. $\bar{l} = 0$), an expression is easier to derive, and since this may, in practice, find useful application, it is given in Appendix 1.

In (2) the quantity S/μ_s represents the volume and hence $1/\mu_s$ represents the depth of radioactive material which in the *absence of internal absorption* would be equivalent to the deposit of infinite depth with absorption. Similarly, $\rho_s S/\mu_s$ is the equivalent mass of material: this is independent of the nature of the deposit since μ_s/ρ_s ($\sim 0{\cdot}06$ for 1 MeV γ energy), the mass absorption coefficient, is practically a constant. The deposit may be defined therefore by the product of N the activity and S the area.

2.3. *Detector response.*—If the flux of a stationary γ-ray field through the detector A is I_s, the detector indicator or signal i may be made proportional to I_s ($= kI_s$). The signal may be registered as a γ-ray count or as a deflexion on a recorder following a d.c. amplifier or ratemeter. When the flux I is varying as in the case of an aircraft moving in the vicinity of a radioactive deposit, the recorded signal will be modified by the time of response of the detector. The differential equation determining the variation of i with time is

$$\frac{di}{dt} + \frac{i}{\tau} = \frac{k}{\tau}\cdot I \qquad (3)$$

where the time constant τ measures the time of response of the detector.

Generally, during aerial prospecting, the aircraft will not pass directly above any deposit. If the nearest approach or minimum range is $\bar{l}_o$ (Fig. 2) then

$$\bar{l} = (\bar{l}_0^2 + v^2t^2)^{\frac{1}{2}} \qquad (4)$$

where $v =$ speed of aircraft
and $t = 0$ when $\bar{l} = \bar{l}_0$

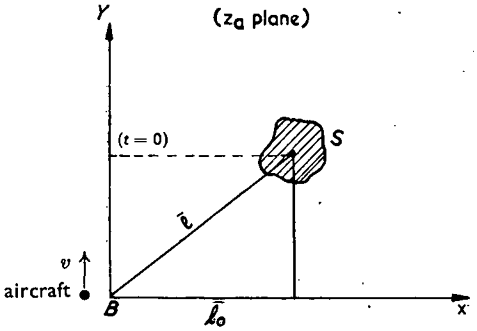

Fig. 2. Minimum range

The peak signal i_{max} is derived in Appendix 2 by substituting from (2) and (4) in (3), integrating and maximizing for t. Thus

$$i_{max} = kI_0\frac{e^{-\mu_a\sqrt{(z_a^2+\bar{l}_0^2)}}}{z_a(z_a^2+\bar{l}_0^2)^{\frac{1}{2}}}\left\{1 - \frac{v^2\tau^2}{z_a^2+\bar{l}_0^2}\,\frac{[1+\mu_a\sqrt{(z_a^2+\bar{l}_0^2)}]}{2}\right\} \qquad (5)$$

where
$$I_0 = \frac{NA\rho_s S}{4\pi\mu_s}$$

The expression in brackets is the factor introduced by the movement of the detector, modifying equation (2).

At $z_a = 500$ ft, $\bar{l}_0 = 0$, $\tau = 1$ sec and $v = 120$ m.p.h. the bracketed expression becomes $1 - 0{\cdot}16$, i.e. the peak signal is reduced to 84% of the stationary value.

2.4. *Performance factor.*—In addition to transient signals due to radioactive anomalies, the detecting apparatus will register continuously an indication, i_b, due to background radioactivity which may have a masking effect on the real signal. The performance of a particular detecting apparatus may be measured in terms of i_{max}/i_b or more appropriately by the ratio R of i_{max} to the amplitude of the statistical variation of i_b, i_{max} and i_b being expressed as counts/unit time. Assuming the background flux to be of random origin the standard deviation of i_b is $\sqrt{(i_b/2\tau)}$. This sets a lower limit to the detectability of i_{max}.

$$\text{Let } R = i_{max}\sqrt{(2\tau/i_b)} \text{ and } i_b = \Sigma\,(kI)_b = k_b I_b$$

where k_b and I_b refer to total background.
Therefore

$$R = i_{max}\sqrt{\frac{2\tau}{k_b I_b}}$$

$$= \frac{k}{\sqrt{k_b}}\sqrt{\frac{2}{I_b}} \cdot I_0 \frac{\epsilon^{-\mu_a\sqrt{(z_a^2+\bar{l}_0^2)}}}{z_a(z_a^2+\bar{l}_0^2)^{\frac{1}{2}}} \cdot \left\{1 - \frac{v^2\tau^2}{z_a^2+\bar{l}_0^2}\,\frac{[1+\mu_a\sqrt{(z_a^2+\bar{l}_0^2)}]}{2}\right\}\sqrt{\tau} \qquad (6)$$

from (5).

It will be profitable to consider the nature of the various quantities that determine the magnitude and behaviour of the performance factor R.

The nature and relative importance of the several components of I_b are discussed in Section 5. For the purposes of the present calculation I_b will be assumed constant in (6).

The quantities k and k_b determine the respective detection efficiencies for signal and total background. k_b is generally not equal to k owing to the diverse origins of I_b, and to the possible dissimilar energy distribution of signal and background γ rays. Choice of the type of detector will be influenced by $k/\sqrt{k_b}$, remembering that k_b may be decreased by auxiliary devices that discriminate against background.

The detector area A (cross-sectional area of counter or chamber) determines with k the overall sensitivity of the apparatus. In practice increase of A is limited only by considerations of space and weight and, indirectly, by serviceability and maintenance problems.

It is seen in (6) that R is dependent upon a function of τ

$$f(\tau) = \left\{1 - \frac{v^2\tau^2}{z_a+\bar{l}_0^2}\,\frac{[1+\mu_a\sqrt{(z_a^2+\bar{l}_0^2)}]}{2}\right\}\sqrt{\tau}$$

The value of τ can be chosen to suit the condition of the experiment. Differentiating with respect to τ gives an optimum value

$$\tau_0 = \frac{(z_a^2+\bar{l}_0^2)^{\frac{1}{2}}}{v}\left\{\frac{2}{5\,[1+\mu_a\sqrt{(z_a^2+\bar{l}_0^2)}]}\right\}^{\frac{1}{2}}.$$

This gives $f(\tau_0) = 0{\cdot}64\,\dfrac{(z_a^2+\bar{l}_0^2)^{\frac{1}{4}}}{v^{\frac{1}{2}}}\,\dfrac{1}{[1+\mu_a\sqrt{(z_a^2+\bar{l}_0^2)}]^{\frac{1}{4}}}$

and hence from (6)

$$R_{max} = \left\{0{\cdot}90 \cdot \frac{kI_0}{\sqrt{k_b}\sqrt{I_b}}\right\} \cdot \frac{\epsilon^{-\mu_a\sqrt{(z_a^2+\bar{l}_0^2)}}}{v^{\frac{1}{2}}z_a(z_a^2+\bar{l}_0^2)^{\frac{1}{4}}}\,\frac{1}{[1+\mu_a\sqrt{(z_a^2+\bar{l}_0^2)}]^{\frac{1}{4}}} \qquad (7)$$

The optimum time constant τ_0 is plotted against altitude in Fig. 3 for different aircraft speeds. The effect of air absorption is demonstrated by the broken curves for $\mu_a = 0$. The variation of R_{max} with speed is illustrated in Fig. 4. Since each speed has its appropriate time constant to give R_{max}, this leads to $\tau_0 \to \infty$ as $v \to 0$ and hence $R_{max} \to \infty$ as $v \to 0$. Fig. 5 shows R_{max} plotted against altitude. In Figs. 4 and 5 the ordinates are independently normalized, and have no practical significance.

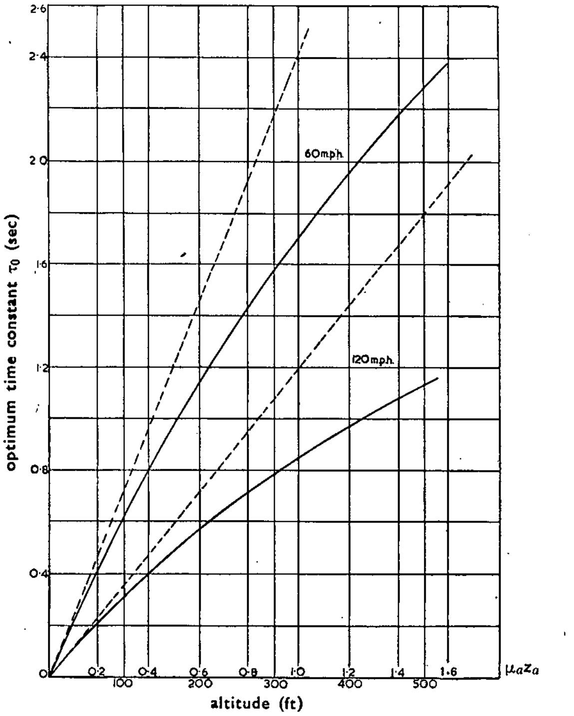

Fig. 3. Optimum time constant against altitude ($\bar{l}_0 = 0$)

$$\tau_0 = \frac{(z_a^2+\bar{l}_0^2)^{\frac{1}{2}}}{v}\left\{\frac{2}{5[1+\mu_a\sqrt{(z_a^2+\bar{l}_0^2)}]}\right\}^{\frac{1}{2}}$$

Minimum range $\bar{l}_0 = 0$ ——— $\mu_a = 0{\cdot}0001$ cm^{-1} - - - - $\mu_a = 0$

2.5. *Conditions of search for minimum deposit.*—The preceding calculations and figures relate to detector response over a known radioactive deposit. To prepare a scheme of aerial prospecting it is necessary to proceed

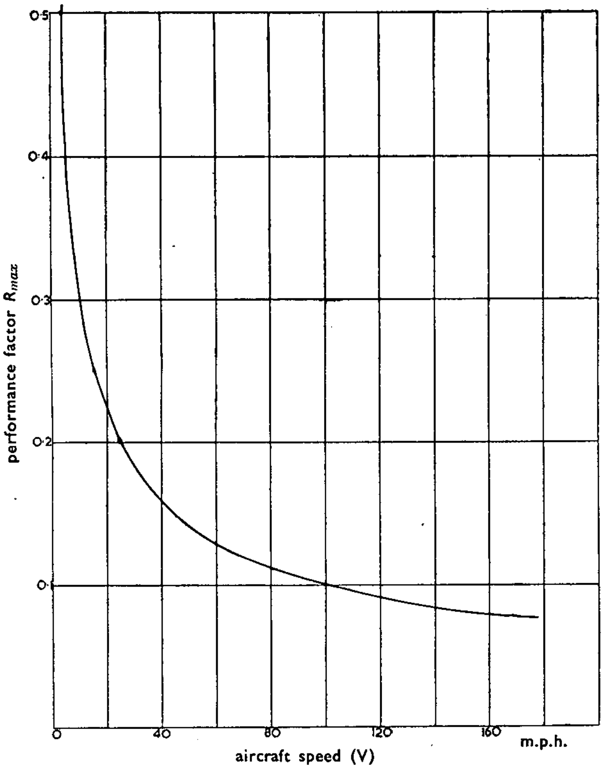

Fig. 4. Performance factor against aircraft speed $R_{max} \propto \frac{1}{v^{\frac{1}{2}}}$

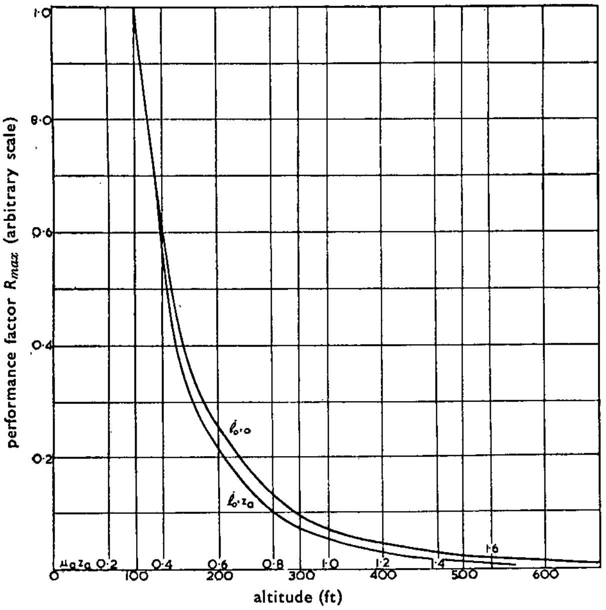

Fig. 5. Performance factor against altitude

$$R_{max} \propto \frac{\epsilon^{-\mu_a\sqrt{(z_a^2 + \bar{l}_0^2)}}}{z_a(z_a^2 + \bar{l}_0^2)^{\frac{1}{4}}\,[1 + \mu_a\sqrt{(z_a^2 + \bar{l}_0^2)}]^{\frac{1}{4}}}$$

$\mu_a = 0{\cdot}0001\ \text{cm}^{-1}$

inversely and investigate the operational conditions that ensure detection of all radioactive deposits above a certain minimum strength. This minimum will be set by geological and economic considerations. The factors influencing the choice of aircraft are discussed in Section 3.2. The plan of flight will depend upon the navigation system employed but will generally consist of traversing the territory by a series of parallel equidistant lanes. Since for a given speed, the time taken to traverse the territory is inversely proportional to the lane width, it is desirable to derive a relation between minimum deposit strength, lane width and performance factor.

Substituting for I_0 from (5) in (7), R_{max} is plotted in Fig. 6 against NS for various values of $\bar{l}_0/z_a$ with $z_a = 500$ ft; $\bar{l}_0$ now represents the half-lane width and NS the strength of a deposit (N = specific activity, S = area of deposit). To give this graph practical value the results of Section 4 are anticipated by drawing in a boundary line defining the limit of detectability as $R_{max} = 3$. Thus the intersection of $R_{max} = 3$ with any $\bar{l}_0/z_a$ curve defines the half-lane width and the deposit strength that is just detectable in mid-lane. The deposit strength is measured practically by the product of concentration, in equivalent percentage by weight of U_3O_8, and area, in square yards. The deposit strengths and lane widths derived in this way represent limiting conditions: points lying above $R_{max} = 3$ refer to conditions of greater detectability.

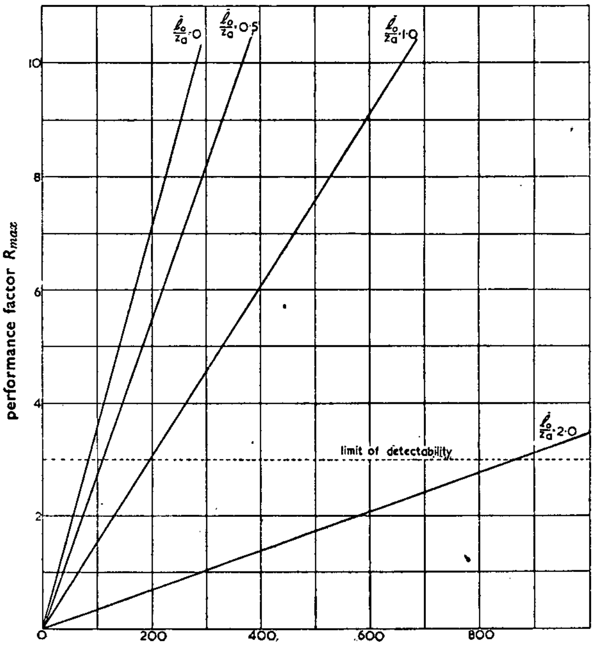

Fig. 6. Performance factor against deposit strength (500 ft)

$$R_{max} \propto \frac{NS\epsilon^{-\mu_a\sqrt{(z_a^2 + \bar{l}_0^2)}}}{z_a(z_a^2 + \bar{l}_0^2)^{\frac{1}{4}}\,[1 + \mu_a\sqrt{(z_a^2 + \bar{l}_0^2)}]^{\frac{1}{4}}}$$

$\mu_a = 0{\cdot}0001\ \text{cm}^{-1} \quad v = 120$ m.p.h.

$2\bar{l}_0$ = lane width

From statistical reasoning[2] the probabilities of a signal deviation greater than 1, 2 and 3 times the standard deviation are respectively, and approximately $\frac{1}{3}$, $\frac{1}{22}$ and $\frac{1}{370}$. Consequently a lower limit of detectability chosen at $R_{max} = 3$ would appear pessimistically high. Practical experience has shown however that this figure is satisfactory and that it allows for the effect of small local variations in background and removes uncertainty in interpretation of records.

Throughout this mathematical assessment of the aerial prospecting problem no attempt is made to account for rapid changes in topography or for the presence of inactive superficial drift masking the radioactive deposit. A few feet of "overburden" will cause severe attenuation of γ intensity. Some slight modification may be caused by the effect of scattering within the deposit and in the atmosphere. Deposit strengths have been regarded in terms of equivalent U_3O_8 concentration: these may be converted to a ThO_2 scale for thorium deposits. The choice of an effective value for μ_a is admittedly controversial, attended as it is by an attempted estimation of several imponderables such as atmospheric scattering, density variations and the mean energy representative of the radioactive γ spectrum. Further information may be derived from data provided by Evans and Evans.(3)

3. APPARATUS

3.1. *Choice of detector.*—Following the argument developed in Section 2.4, it is clear that γ *signal* sensitivity is an incomplete criterion of the efficacy of a detecting instrument. Instead a factor $k/\sqrt{k_b}$ is introduced to account also for background sensitivity. Ionization chambers give undesirable prominence to the intensely ionizing particles and showers forming the cosmic component of background. Geiger counters register cosmic and γ events with equal prominence and further, it is possible to inter-connect a bundle of counters so that most of the penetrating cosmic component is cancelled (Section 5.1). The γ signal intensity and remaining γ component of background are counted with a Geiger counter efficiency, of $\sim 0{\cdot}003$, compared with ~ 1 for cosmic rays. Scintillation counters seem capable of an increase of as much as 50 times in efficiency if γ counting, thereby providing virtual elimination of the penetrating cosmic component. The necessity for the maintenance of high stability in the amplifier and discriminator circuits associated with a scintillation counter detracts somewhat from this improvement in efficiency.

The order of merit, measured in terms of $k/\sqrt{k_b}$ is then, scintillation counter, Geiger counter, ionization chamber. For the work described in this paper the Geiger counter was preferred to the then incompletely developed scintillation counter.

3.2. *Choice of Aircraft.*—Consideration of (7) or Figs. 4 and 5, when attempting to obtain the best performance, leads to the choice of an aircraft having the lowest possible cruising speed and safe operating height. Such a specification is probably best satisfied by the helicopter and this may well be the most suitable choice under certain conditions. The desirable minima of speed and altitude must be reconciled with the more practical consideration of:—

(i) time spent over survey increases with decreasing cruising speed;

(ii) local topography—rapidly varying ground level raises safe operating altitude;

(iii) space for installation of detecting equipment and possible navigational aids;

(iv) endurance—avoidance of frequent stops for refuelling favours large petrol capacity, hence large aircraft;

(v) aircraft maintenance and servicing;

and (vi) availability.

Availability will have over-riding importance when Service aircraft or aircraft attached to the Geological Department, engaged on transport, magnetometer or photographic surveys already operate in or near the area to be surveyed.

3.3. *Aerial survey equipment type* 1073*A*.—The equipment consists of an assembly of 49 Geiger tubes with quenching, anti-coincidence and ratemeter circuits, pen recorder and a power pack drawing current from a 24 V supply. Fig. 7 is a schematic diagram of the circuit.

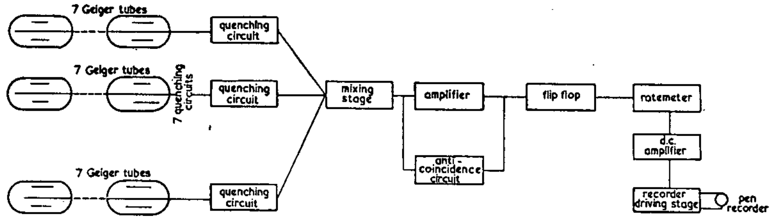

Fig. 7. Aerial survey equipment type 1073A. Schematic diagram

Geiger tubes: The Geiger tubes (type GM1B) have graphite cathodes of length 63 cm and diameter 3·4 cm and are filled with an argon-ethyl bromide low temperature mixture at pressures of 9 cm and 1 cm respectively. The tubes are arranged horizontally in 7 rows of 7, the anodes, spaced at 4·3 cm, being connected in staggered columns of 7, each column connected to a quenching circuit.

Quenching circuits: The quenching circuits have quench periods of 500 μS which is sufficient to suppress any possible spurious counting from the Geiger tubes.

Mixing circuit: The mixing circuit combines pulses from the 7 quenching circuits. Any pulses occurring simultaneously (within $6\,\mu S$), i.e. coincidence pulses due to penetrating cosmic rays initiating tubes in 2 or more columns, combine and produce additive pulses of magnitude greater than single amplitude. Pulses of single amplitude are due to normal γ initiation. The rate of accidental coincidence is small at the γ count rates experienced.

Anti-coincidence circuit: The anti-coincidence circuit discriminates against pulses of greater than single amplitude and hence against cosmic rays.

Ratemeter circuit: The ratemeter circuit converts the Geiger pulse rate into a rate voltage. Sensitivity may be adjusted over a nominal range of 1 : 10 : 100 by selection of appropriate condensers. Alternative time constants of 1·5 and 0·75 sec are available. Time constant and sensitivity adjustments are made by relays switched externally. Feed-back introduces non-linearity into the recorder deflexion-count relation to prevent overloading at high γ intensities.

Recorder: A robust recorder of the single channel type by Kelvin-Hughes Ltd. uses electrical marking of facsimile paper at a paper speed of 0·25 cm/sec. The centre-tapped coil has a resistance of 5 000 Ω, sensitivity of 0·72 mm/V and resonant frequency of 30 c/s. Time marking is introduced through an auxiliary fixed pen from a half-second clock. On the most sensitive range the background is automatically offset by a pre-set amount to allow a full recorder scale for signal deflection. On the other ranges the background indication is included in the recorder deflexion and forms a useful overall calibration.

Power supply: 20 A are required at 24 V d.c. This is converted by motor generator to 80 V at 1 600 c/s.

Size and weight: 4 ft 6 in × 1 ft × 1 ft: 150 lb.

Aircraft: The aircraft used for this work was a standard R.A.F. Anson—a twin-engined monoplane, crew capacity 6, cruising speed 120 m.p.h. and endurance 4½ h.

4. FLIGHT RESULTS

The aerial prospecting equipment has been tested over a high grade artificial "deposit" of small area and over more extensive low grade natural deposits. The experimental flying programme was planned as a comprehensive check of the preceding theoretical results. Although flying was discontinued before the programme was completed, sufficient reliable data were obtained to set a practical scale for the calculations and graphs derived in Section 2.

4.1. *Artificial deposit.*—Ten cylindrical containers of pitch-blende (60% U_3O_8) each half-filled and containing 1 cwt of ore were placed horizontally on the aerodrome to form an approximately square ore surface at ground level of effectively infinite depth ($\not<$ 10 cm) over an area of 1·4 yd^2. Some specimen records are reproduced in Fig. 8 which demonstrates the variation, with time constant, of signal and background deviation at constant altitude and speed. The detectability level of Fig. 6 is fixed by reference to results obtained over the artificial deposit (concentration × area = 84). Altitudes were

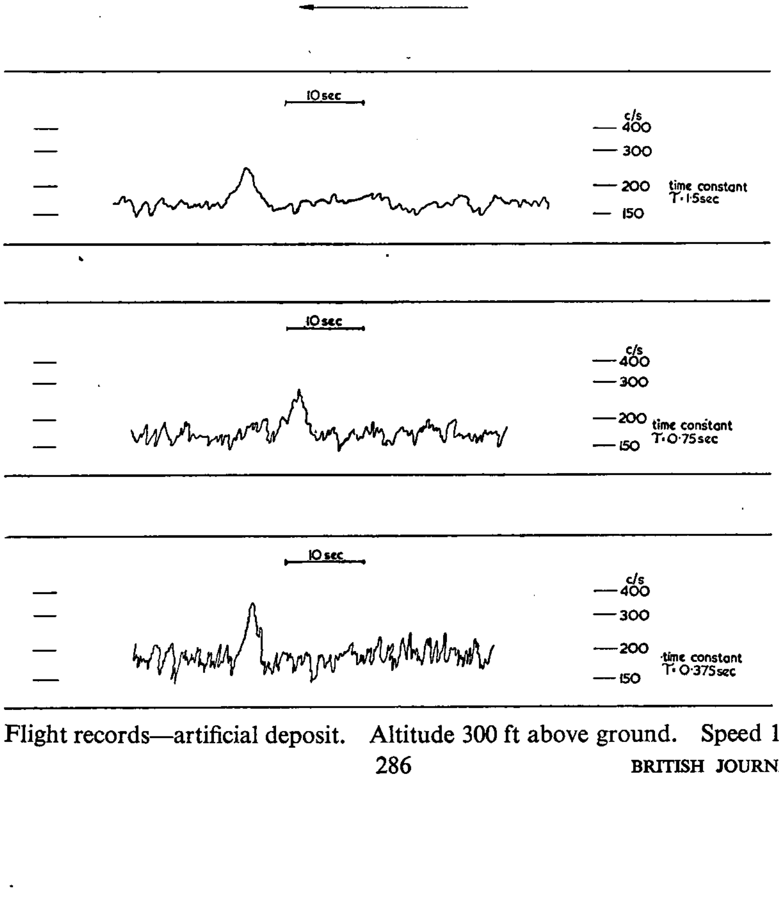

Fig. 8. Flight records—artificial deposit. Altitude 300 ft above ground. Speed 115 m.p.h.

measured by altimeter, checked at ground level at the deposit before and after each series of flights; speeds measured by the aircraft instrument were corrected for wind velocity to give true ground speed; flight path was determined visually or with the Decca Navigator.

4.2. *Natural deposits.*—A series of flights was made over natural deposits of uranium ore. Peak recorder deflexions over a typical natural deposit are plotted against altitude in Fig. 9 for signal and *mean* total background. It is interesting to note the steep rise of signal with decreasing altitude and the constancy of background deflexion from 200 to 2 000 ft. The rise in background below 200 ft is abnormal and due to extensive contamination of the country surrounding the deposit.

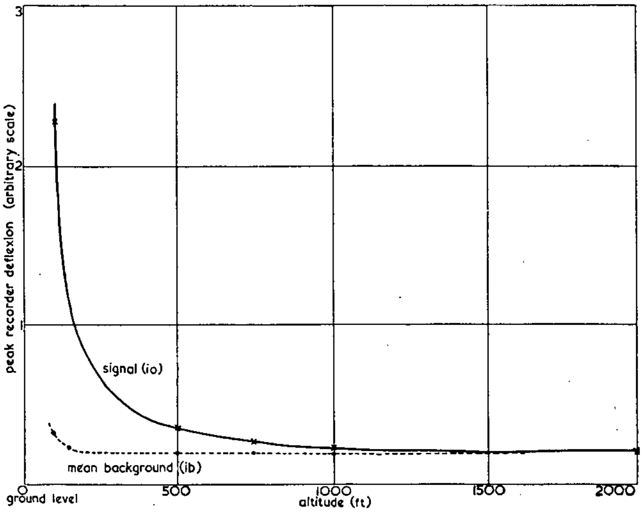

Fig. 9. Measured recorder deflexion against altitude—typical natural deposit. Speed 138 m.p.h. time constant 3 sec

Fair agreement was shown between the results for these deposits of large linear dimensions and the theory of Section 2, which applies strictly only to deposits of small area. Some typical measurements over the artificial deposit are shown in Table 1, together with calculated figures, based on these measurements, and derived from Figs 4, 5 and 6

5. BACKGROUND ACTIVITY

It was shown in Section 2.4 how the performance factor R is influenced by the background flux I_b and the total background detection efficiency k_b. It is of interest to consider the nature of I_b and how R may be increased by reducing k_b. The total background consists of four components: that due to cosmic activity I_c; γ activity of the earth's surface I_e; γ activity of the atmosphere I_a; and γ active contamination of equipment and aircraft I_x. Thus

$$\begin{aligned} i_b &= k_b I_b \\ &= k_c I_c + k_e I_e + k_a I_a + k_x I_x \end{aligned}$$

Representative values of the various Geiger detection efficiencies are

$$k_c \sim 1$$
$$k_e, k_a, k_x \sim 0{\cdot}003$$

5.1. *Cosmic activity.*—Cosmic activity is due to a complex radiation composed of a penetrating or *hard* part consisting mainly of mesons and possibly some very energetic electrons and photons together with a comparatively absorbable or *soft* part of electrons and photons. The total omni-directional cosmic intensity/cm^2 horizontal cross-sectional area/min is about 1·2.⁽⁴⁾ This applies at sea level in geomagnetic latitudes greater than 45°. It is estimated that the hard part represents $\frac{2}{3}$ of the total intensity under these circumstances, the separation of the hard from the soft being defined by the arbitrary absorption criterion of 10 cm of lead.

Unlike normal γ radiation, the majority of the cosmic rays are each capable of initiating several of a bundle of Geiger tubes. Then if the average number of tubes operated, effectively simultaneously, by a single cosmic particle is n, the detection efficiency per unit area for the whole bundle is reduced to k_c/n. n is a function of the total number and closeness of tubes in the bundle. In addition, k_c may be further reduced by an anti-coincidence arrangement as described in Section 3.3. In this case all cosmic particles registering on more than

Table 1. *Flight results*

		area sq yd	*concentration % U_3O_8*	*altitude ft*	*speed m.p.h.*	R_{max}	*lane width ($2\bar{l}_0$) ft*	*remarks*
		measured						
1.	*Artificial deposit*	1·4	60	500	120	3	overhead	just detectable
2.		1·4	60	300	120	12	overhead	
		calculated						
3.		420	0·2	500	120	3	overhead	just detectable
4.		420	0·2	300	120	12	overhead	
5.		3·3	60	500	120	3	1 000	just detectable
6.		1 000	0·2	500	120	3	1 000	just detectable
7.		0·9	60	300	60	3	600	just detectable
8.		270	0·2	300	60	3	600	just detectable
9.		7·5	0·2	100	60	3	overhead	just detectable

one tube are eliminated and only those registering singly or by grazing incidence at the corners of the bundle are counted. The total "cosmic elimination efficiency," taking into account the soft part, of the 49 tube assembly has been estimated with some uncertainty as 60% including some 7% due to the anti-coincidence circuit alone.

The cosmic intensity will increase by approximately 9%⁽⁵⁾ from ground level to 1 000 ft altitude, i.e. for a decrease in barometric pressure of about 1 inch of mercury.

5.2. *Earth activity.*—The background flux I_e is due to γ-activity arising from uranium, thorium and potassium present generally in the earth's surface. The content varies with geological conditions, 0·001% equivalent U_3O_8 being a typical concentration. The ground level γ-intensity corresponding to this concentration would be of the order of 200/cm² cross-sectional area/min and produces 0·6 counts/cm² cross-sectional area/min in a Geiger tube of efficiency 0·003.

The theoretical variation with altitude is calculated in Appendix 3 and shown graphically in Fig. 10. The striking feature of this theoretical curve is the rapid decrease exhibited with increase of altitude. At 500 ft the flux is less than $\frac{1}{10}$ of the ground level value.

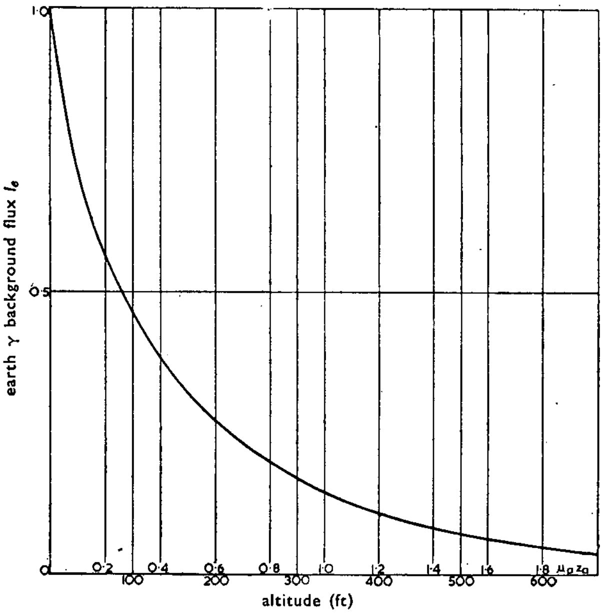

Fig. 10. Earth γ background flux against altitude (theoretical)

$$I_e = \frac{N_e A \rho_s}{2\mu_s} \int_1^\infty \frac{1}{q^2} \epsilon^{-\mu_a z_a q}\, dq$$

$$\mu_a = 0\cdot0001 \text{ cm}^{-1}$$

5.3. *Atmospheric activity.*—A component of background intensity may be tentatively attributed to the activity of the emanations diffusing from the pervading radioactive content of the earth's surface. The mechanism of this diffusion effect has been described by Hess:⁽⁶⁾ it is reasonable to assume a fairly uniform atmospheric distribution of active material, mainly of radon and its products, over the operational range of aerial prospecting altitudes. By calculation similar to that of Appendix 3 it is possible to demonstrate a variation with altitude of atmospheric γ-flux I_a complementary to that for I_e. The value of I_a at 500 ft is nearly double that at ground level, owing to the contribution from below as well as above. A typical value for the mean radioactivity of the atmosphere is 3×10^{-13} c/l. The corresponding γ-ray intensity at ground level due to this atmospheric activity is only 10/cm² cross-sectional area/min, i.e. 0·03 counts/cm²/min with a Geiger counter efficiency of 0·003.

5.4. *Contamination activity.*—Although for normal purposes γ-activity due to contamination of equipment may be neglected, these aerial survey measurements are made at such low intensity levels that it is important to ensure no contact with radioactive materials during manufacture and assembly of the equipment. As a practical example of the undesirability of such contamination, activity was located after considerable difficulty within the glass envelopes of a batch of commercially manufactured Geiger tubes. The spurious increase in background indication was in some cases equivalent to an earth concentration of 0·002% U_3O_8. There was also trouble from luminous paint on the aircraft instrument dials. In the Anson aircraft used for this work the background intensity was appreciably enhanced in the vicinity of the pilot's seat. However the equipment could be suitably sited and where necessary screened by lead from any undesirable external influence of this type.

5.5. *Discussion of background factors.*—From the preceding estimates of background intensities and variations with altitude, it is possible to compare the total background count rate for the 49 Geiger tube equipment at ground level and at a typical operating altitude. Taking account of the increase with altitude of the residual uneliminated cosmic component, decrease of the earth's surface component, increase of a possible atmospheric component and ignoring the effect of any contamination activity, the total background count rate i_b at 500 ft over a surface containing 0·001% equivalent U_3O_8 should be approximately $\frac{2}{3}$ of the ground level value, and is predominantly cosmic in composition. Despite uncertainty over the response of a scintillation counter to the soft part of the cosmic component, it is safe to conclude that for this type of detector the γ background components form the major part of i_b at ground level and 500 ft. Assuming an improvement in γ-ray detection efficiency of 50 times that of a Geiger counter, the improvement in performance for a given bulk, having regard to the ratio $k/\sqrt{k_b}$, should be about 7 times. However, owing to the difficulty of producing large efficient volumes of a scintillation material such as napthalene, anthracene, sodium iodide, etc., this increase in performance may be limited in practice to about 3 times.

6. CONCLUSIONS

It has been demonstrated that, in the absence of overburden masking the radiation, it is possible to detect a radioactive deposit of concentration (% U_3O_8) times area (sq yd) factor of 84 with a 49 Geiger tube equipment flying at an altitude of 500 ft and speed of 120 m.p.h. By calculation it is possible to extend the measured performance to cover the full operational range likely to be encountered in a programme of aerial prospecting. The equipment has proved highly reliable under flight conditions of normal severity. Automatic operation with pilot control and a signal warning system could be introduced to simplify use of the equipment.

Scintillation counter: The potential importance as a γ-ray detector of the scintillation counter has been indicated. It is expected that compared with a Geiger equipment an improvement in performance of about 3 times could be achieved.

Navigation: Some form of navigational aid is desirable in order to ensure both an accurate fix of any discovery and complete coverage, without overlapping, of the whole survey area. Simple methods such as map reading and photography may suffice: the improved accuracy and reliability of radio aids such as "Gee" or "Decca" may be offset by additional expense and complexity.

7. ACKNOWLEDGMENTS

Acknowledgments are due to Mr. F. H. Wells and Mr. W. H. Rann for contributions in design and construction of equipment, to Dr. J. Howlett for suggesting the treatment of Appendix I, to Mr. C. Campbell (Geological Survey) for geological advice and to the Royal Air Force who provided flying facilities. The paper is published by permission of the Director of the Atomic Energy Research Establishment, Harwell.

8. REFERENCES

(1) Heitler, W. *The Quantum Theory of Radiation* (London: Oxford University Press, 1944.)

(2) Levy, H., and Roth, L. *Elements of Probability.* (London: Oxford University Press, 1936.)

(3) Evans, R. D., and Evans, R. O. *Rev. Mod. Phys.*, **20**, p. 305 (1948).

(4) Montgomery, D. J. X. *Cosmic Ray Physics.* (Princeton: Princeton University Press, 1949.)

(5) Duperier, A. *Nature, Lond.*, **153**, p. 529 (1944).

(6) Hess, V. F. *Electrical Conductivity of the Atmosphere and its Causes.* (London: Constable and Co., Ltd., 1928.)

APPENDIX I

CALCULATION OF γ-RAY FLUX

The essence of the calculation is the computation of the integral

$$J = \int_V \frac{1}{r^2} \epsilon^{-\mu_s(r-r_a)}\, \epsilon^{-\mu_a r_a} dV$$

over the whole deposit defined in Section 2.2 and Fig. 1.

i.e.
$$J = \int_S \int_{z=z_a}^{\infty} \epsilon^{(\mu_s - \mu_a)r_a} \cdot \frac{\epsilon^{-\mu_s r}}{r^2}\, dS \,.\, dz \qquad (1)$$

Since $z - z_a$, the operative depth of the deposit, is of the order of $1/\mu_s$ and can be shown to be at least 100 times smaller than z for normal operational altitudes, e may be neglected in comparison with l. Then without appreciable error

$$r_a^2 = z_a^2 + l^2$$

Substituting in (1)

$$J = \int_S \epsilon^{(\mu_s - \mu_a)\sqrt{(l^2+z_a^2)}} \int_{z_a}^{\infty} \frac{\epsilon^{-\mu_s\sqrt{(l^2+z^2)}}}{l_2 + z_2}\, dz \,.\, dS \qquad (2)$$

Considering the integration with respect to z, putting $l^2 + z^2 = p^2$, and expanding,

$$J_z = \int_{p=\sqrt{(l^2+z_a^2)}}^{\infty} \frac{\epsilon^{-\mu_s p}}{p^2} \left(1 + \tfrac{1}{2}\frac{l^2}{p^2} + \tfrac{3}{8}\frac{l^4}{p^4} + \ldots\right) dp$$

As $p^2 > l^2$, the expansion converges and the general term is

$$\int_{p=\sqrt{(l^2+z_a^2)}}^{\infty} \frac{\epsilon^{-\mu_s p}}{p^n}\, dp$$
$$= \frac{\epsilon^{-\mu_s\sqrt{(l^2+z_a^2)}}}{\mu_s\sqrt{(l^2+z_a^2)^n}} \left[1 - \frac{n}{\mu_s\sqrt{(l^2+z_a^2)}} + \frac{n(n+1)}{\mu_s^2(l^2+z_a^2)} \cdots\right]$$
$$= \frac{\epsilon^{-\mu_s\sqrt{(l^2+z_a^2)}}}{\mu_s\sqrt{(l^2+z_a^2)^n}}$$

with a relative error given by the first term neglected, viz.

$$\frac{n}{\mu_s\sqrt{(l^2+z_a^2)}}$$

Hence (except for $\dfrac{l}{z_a} \gg 1$)

$$J_z = \frac{1}{\mu_s} \cdot \frac{\epsilon^{-\mu_s\sqrt{(l^2+z_a^2)}}}{l^2 + z_a^2} \left[1 + \frac{1}{2}\frac{l^2}{(l^2+z_a^2)} + \frac{3}{8}\frac{l^4}{(l^2+z_a^2)^2} + \ldots\right]$$
$$= \frac{1}{\mu_s} \cdot \frac{\epsilon^{-\mu_s\sqrt{(l^2+z_a^2)}}}{z_a\sqrt{(l^2+z_a^2)}}$$

with an overall relative error of order $\dfrac{1}{\mu_s\sqrt{(l^2+z_a^2)}},$ i.e. not greater than $\dfrac{1}{\mu_s z_a}$. Taking $\mu_s = 0 \cdot 12\ \text{cm}^{-1}$ and $z_a = 100$ ft, $\dfrac{1}{\mu_s z_a} \sim \dfrac{1}{360,}$ i.e. the error is negligible for typical values. The total integral (2) becomes

$$J = \frac{1}{\mu_s z_a} \int \frac{\epsilon^{-\mu_a\sqrt{(l^2+z_a^2)}}}{\sqrt{(l^2+z_a^2)}}\, dS \qquad (3)$$

Except for special cases (3) may not be integrated directly but provided the linear dimensions of S are small compared with z_a, the quantity $\sqrt{(l^2+z_a^2)}$ and hence J will vary little over the surface area S. It is possible to select a mean range $\bar{l}$ for the whole surface such that

$$J^1 = \frac{S\, \epsilon^{-\mu_a\sqrt{(\bar{l}^2+z_a^2)}}}{\mu_s z_a\sqrt{(\bar{l}^2+z_a^2)}} \qquad (4)$$

The closeness of this approximation may be indicated by the direct integration of (3) for the particular case of the detector situated vertically above the centre of a circular deposit area of diameter cz_a: this may be compared with the approximate form (4) to give the ratio of the approximate and exact maximum intensities. Writing (3) in polar co-ordinates

$$\mu_s z_a \, . \, J = 2\int_0^{\pi}\int_0^{\frac{cz_a}{2}} \frac{\epsilon^{-\mu_a\sqrt{(l^2+z_a^2)}}}{\sqrt{(l^2+z_a^2)}}\, l\, dl\, d\phi$$

$$= 2\pi\int_0^{\frac{cz_a}{2}} \frac{\epsilon^{-\mu_a\sqrt{(l^2+z_a^2)}}}{\sqrt{(l^2+z_a^2)}}\, l\, dl$$

$$= -\frac{2\pi}{\mu_a}\Big[\epsilon^{-\mu_a\sqrt{(l^2+z_a^2)}}\Big]_0^{\frac{cz_a}{2}}$$

$$= \frac{2\pi}{\mu_a}\epsilon^{-\mu_a z_a}\left[1 - \epsilon^{-\mu_a z_a\left\{\sqrt{\left(1+\frac{c^2}{4}\right)}-1\right\}}\right]$$

Also from (4), putting $S = \dfrac{\pi c^2 z_a^2}{4}$ and $\bar{l} = 0$

$$\mu_s\, z_a \cdot J^1 = \frac{\pi c^2\, z_a}{4} \cdot \epsilon^{-\mu_a z_a}$$

$$\therefore \frac{J^1}{J} = \frac{\mu_a\, z_a}{8} \cdot \frac{c^2}{1-\epsilon^{-\mu_a z_a\left\{\sqrt{\left(1+\frac{c^2}{4}\right)}-1\right\}}}$$

After expansion and to a first approximation,

$$\frac{J^1}{J} \sim 1 + \frac{c^2\mu_a z_a}{16}$$

APPENDIX 2

CALCULATION OF DETECTOR RESPONSE

The detector circuit may be simulated electrically by a parallel combination of resistance and capacity.

Thus it can be shown that, if I is the instantaneous γ flux through the detector, the indicated or recorded current i is given by

$$\frac{di}{dt} + \frac{i}{\tau} = \frac{k}{\tau} \, . \, I \qquad (1)$$

where τ is the time constant of the detector circuit.

If $t = 0$ when the aircraft is at the minimum range $\bar{l} = \bar{l}_0$, integration of (1) gives,

$$i = \frac{k}{\tau}\epsilon^{-\frac{t}{\tau}}\left(\int_{-\infty}^{t} \epsilon^{\frac{t}{\tau}} \, . \, I\, dt\right) \qquad (2)$$

From Fig. 2 the mean range $\bar{l}$ may be written in terms of t

$\bar{l} = \sqrt{(\bar{l}_0^2 + v^2t^2)}$ where $\bar{l}_0$ = minimum range

v = aircraft speed

Substituting for $\bar{l}$ in (2) of Section 2.2, and then for I in (2) (Appendix 2).

$$i = \frac{k}{\tau} I_0 \frac{\epsilon^{-\frac{t}{\tau}}}{z_a} \int_{-\infty}^{t} \epsilon^{t/\tau} \cdot \frac{\epsilon^{-\mu_a\sqrt{(z_a^2+\bar{l}_0^2+v^2t^2)}}}{\sqrt{(z_a^2+\bar{l}_0^2+v^2\,t^2)}}\, dt \qquad (3)$$

where $I_0 = \dfrac{NA\rho_s S}{4\pi\mu_s}$.

This integral may be expanded (Maclaurin) in powers of t^2 thus

$$J_t = \int_{-\infty}^{t} \epsilon^{\frac{t}{\tau}} \cdot \frac{\epsilon^{-\mu_a\sqrt{(z_a^2+\bar{l}_0^2+v^2t^2)}}}{\sqrt{(z_a^2+\bar{l}_0^2+v^2\,t^2)}}\, dt$$

$$= \frac{\epsilon^{-\mu_a\sqrt{(z_a^2+\bar{l}_0^2)}}}{\sqrt{(z_a^2+\bar{l}_0^2)}}\int_{-\infty}^{t} \epsilon^{t/\tau}\,(1 - at^2 + b\,t^4\,\ldots)dt$$

where $a = \dfrac{[1+\mu_a\sqrt{(z_a^2+\bar{l}_0^2)}]v^2}{2(z_a^2+\bar{l}_0^2)}$,

$$b = \frac{[3+3\mu_a\sqrt{(z_a^2+\bar{l}_0^2)}+\mu_a^2(z_a^2+\bar{l}_0^2)]\,v^4}{8(z_a^2+\bar{l}_0^2)^2}$$

The expansion may be integrated term by term. To preserve analytical form and avoid numerical computation, terms above t^2 may be ignored, producing in the vicinity of $t = 0$ a fair parabolic approximation to I.

i.e. $J_t \sim \dfrac{\epsilon^{-\mu_a\sqrt{(z_a^2+\bar{l}_0^2)}}}{\sqrt{(z_a^2+\bar{l}_0^2)}} \cdot \tau\,\epsilon^{\frac{t}{\tau}}\,[1 - a(t^2 - 2t\tau + 2\tau^2)]$

From (3)

$$i = kI_0 \cdot \frac{\epsilon^{-\mu_a\sqrt{(z_a^2+\bar{l}^2)}}}{z_a\sqrt{(z_a^2+\bar{l}_0^2)}} \cdot [1 - a(t^2 - 2t\tau + 2\tau^2)]$$

By differentiating *w.r.t.* t and equating to zero it can be shown that the maximum value of i occurs at $t = \tau$

i.e.

$$i_{max} = kI_0\frac{\epsilon^{-\mu_a\sqrt{(z_a^2+\bar{l}_0^2)}}}{z_a\sqrt{(z_a^2+\bar{l}_0^2)}}(1 - a\tau^2)$$

$$= kI_0\frac{\epsilon^{-\mu_a\sqrt{(z_a^2+\bar{l}_0^2)}}}{z_a\sqrt{(z_a^2+\bar{l}_0^2)}}\left\{1 - \frac{v^2\tau^2}{2}\,\frac{[1+\mu_a\sqrt{(z_a^2+\bar{l}_0^2)}]}{z_a^2+\bar{l}_0^2}\right\}$$

APPENDIX 3

CALCULATION OF γ-RAY BACKGROUND FLUX

Following Section 2.2 the γ-ray background flux due to earth activity I_e may be written

$$I_e = \frac{N_e A\rho_s}{4\pi}\int_v \frac{1}{r^2}\,\epsilon^{-\mu_s(r-r_a)}\,\epsilon^{-\mu_a r_a}\,dV$$

where N_e = γ activity of earth/unit mass/unit time.

ρ_s = density of earth.

The integration now extends over a "deposit" of infinite dimensions. Transforming to spherical co-ordinates ($dV = r^2\sin\theta dr\, d\phi\, d\theta$),

$$I_e = \frac{N_e A \rho_s}{4\pi} \int_0^{\frac{\pi}{2}} \int_0^{2\pi} \int_{z_a \sec\theta}^{\infty} \sin\theta\, \epsilon^{-\mu_s(r - z_a \sec\theta)}\, \epsilon^{-\mu_a z_a \sec\theta}\, dr\, d\phi\, d\theta$$

$$= \frac{N_e A \rho_s}{4\pi\mu_s} \int_0^{\frac{\pi}{2}} \int_0^{2\pi} \sin\theta\, \epsilon^{-\mu_a z_a \sec\theta}\, d\phi\, d\theta$$

$$= \frac{N_e A \rho_s}{2\mu_s} \int_0^{\frac{\pi}{2}} \sin\theta\, \epsilon^{-\mu_a z_a \sec\theta}\, d\theta$$

Putting $q = \sec\theta$

$$I_e = \frac{N_e A \rho_s}{2\mu_s} \int_1^{\infty} \frac{1}{q^2} \epsilon^{-\mu_a z_a q}\, dq$$

This final integral may be evaluated from mathematical tables and is plotted as a function of z_a in Fig. 10.

Putting $z_a = 0$, the ground level value for I_e,

$$I_{eo} = \frac{N_e A \rho_s}{2\mu_s}$$

In like manner the γ background flux due to atmospheric activity is given by

$$I_a = \frac{N_a A}{\mu_a}\left(1 - \tfrac{1}{2} \int_1^{\infty} \frac{1}{q^2} \epsilon^{-\mu_a z_a q}\, dq\right)$$

and the ground level value by

$$I_{ao} = \frac{N_a A}{2\mu_a}$$

where N_a is the γ activity of the atmosphere/unit volume/unit time and is assumed to be independent of z_a.

A three dimensional electrical potential analyser

By S. C. Redshaw, M.Sc., Ph.D., M.I.C.E., F.R.Aë.S., Boulton Paul Aircraft Ltd *

[*Paper first received* 16 *April*, 1951, *and in final form* 18 *May*, 1951]

An electrical potential analyser has been designed and constructed for the purpose of solving the three dimensional form of Laplace's equation, which has such wide uses in connexion with potential theory. The basic idea of the analyser is that, by means of an electrical analogy, a pure resistance network is used to solve the finite difference form of the potential equation, and a novel form of construction is employed which enables readings of a high order of accuracy to be obtained by the use of the instrument. The analyser has been used to solve several cases of potential flow around aeroplane wings of unconventional shape, but other problems involving the solution of Laplace's equation could equally well be solved by the use of the apparatus.

INTRODUCTION

There are numerous problems in mathematical physics which involve the solution of Laplace's equation in two or three dimensions. In only a few cases is it possible to obtain a mathematical solution to the problem and recourse is usually made to some approximate means, such as the Relaxation Method,(1) in order to obtain a practical solution. As an alternative to a computational method electrical analogies have been devised which have been successfully used for the solution of two dimensional problems in potential theory.(2,3,4,5.) Following the use of a two dimensional electrical potential analyser(6) the possibility of constructing a three dimensional instrument was manifest and the present paper describes the design, construction and use of an analyser which was built for the principal purpose of investigating the potential fluid flow around aeroplane wings of unconventional shape. It will be appreciated that the use of the apparatus is not confined to problems of fluid flow but can equally well be used for any problem involving the solution of Laplace's equation.

THE THEORY OF THE INSTRUMENT

Mathematical Theory.—Laplace's equation for three dimensional potential flow in Cartesian co-ordinates is

$$\frac{\partial^2\phi}{\partial x^2} + \frac{\partial^2\phi}{\partial y^2} + \frac{\partial^2\phi}{\partial z^2} = 0. \qquad (1)$$

The mathematical solution of this equation involves the obtaining of an analytical expression for the function ϕ over the domain in question, while at the same time satisfying the boundary conditions; only in a few simple cases is a mathematical solution possible. An approximate solution may be obtained by the use of the relaxation technique, the accuracy of the solution depending on the size of the relaxation net used. The labour involved in the use of the relation technique can be very considerable and, in the case of many three dimensional problems, almost prohibitive. The electrical potential analyser possesses the important advantage over the relaxation process in that it provides the final answer to the problem when the electrical potentials have been measured at the nodes of the net, whereas in the relaxation method the solution is only obtained after a series of net relaxations. In addition, only that portion of the net which is of interest need be probed. In both methods

---

* Now at Department of Civil Engineering, University of Birmingham.

the first step is to set up the equation to be solved in finite difference form, thus equation (1) becomes

$$6\phi_0 - \sum_{n=1}^{n=6} \phi_n = 0 \qquad (2)$$

where ϕ_0 is the value of the required function at a node of a cubical mesh and $\phi_1, \phi_2 \dots \phi_6$ are the values of the function at the six surrounding nodal points. A cubical mesh has been used, in the present instance, for general convenience but other mesh forms are possible.

Electrical Theory.—Consider a cubical mesh of resistors where r is the value of each resistor, and $i_2 \dots i_6$ the currents flowing in the six arms of the mesh from the points 1, 2 . . . 6 to the node 0. If $\phi_0\, \phi_1 \dots \phi_6$ are the values of the electrical potentials at the nodes considered then, by Ohm's law,

$$6\phi_0 = \sum_{n=1}^{n=6} \phi_n = \mathrm{r}(i_1 + i_2 + \dots + i_6) \qquad (3)$$

but by Kirchoff's first law the sum of the currents at any junction must equal zero and therefore equation (3) reduces to equation (2), the finite difference form of equation (1).

THE DESIGN AND CONSTRUCTION OF THE ANALYSER

From the foregoing argument it will be seen that to provide an electrical analogue to the finite difference form of Laplace's equation it is necessary to provide a mesh of electrical resistors. In the previous two dimensional analyser the mesh arms were composed of wire resistance strain gauges, but this would be too costly except for a small instrument, apart from the fact that it would be impossible to obtain strain gauges sufficiently closely matched in resistance. Precision carbon resistances were considered but were discarded because although they might be closely matched, their resistance values might not be sufficiently stable, and the cost of obtaining them to close resistance limits would have been too high.

In order to provide a suitable resistor a considerable amount of development work was undertaken by Boulton Paul Aircraft Ltd. and British Celanese Ltd. and, as a result, a form of woven resistor was satisfactorily developed. The resistor was formed by weaving a 1-in wide ribbon from 47 s.w.g. Minalpha wire and silk, the warp was composed of silk and the weft of wire, woven in such a manner that a loop was formed every half inch on one side of the ribbon. Sheaths were moulded from Xylonite and tags were riveted to these sheaths at half-inch intervals, the wire loops from the ribbon being soldered to the tags and a cover cemented to the sheath for protection. Series resistance elements consisting of twenty-five units were constructed in this manner. Minalpha wire possesses a negligible temperature coefficient of resistance and is extremely suitable for precision resistors while the accuracy with which the ribbon could be woven ensured a tolerance of ± 1% between individual resistance units which had a nominal resistance of 200 Ω.

The analyser was designed to provide nine tiers, each tier being composed of a 25 × 25 square array of points. Fig. 1 shows a general view of the instrument. An insulated panel was drilled to receive an array of plug sockets at a half-inch pitch, each socket had bolted to it, on the back of the panel, a metal stirrup and to these stirrups were attached the twenty-five unit resistance elements. Every socket on each tier was connected to

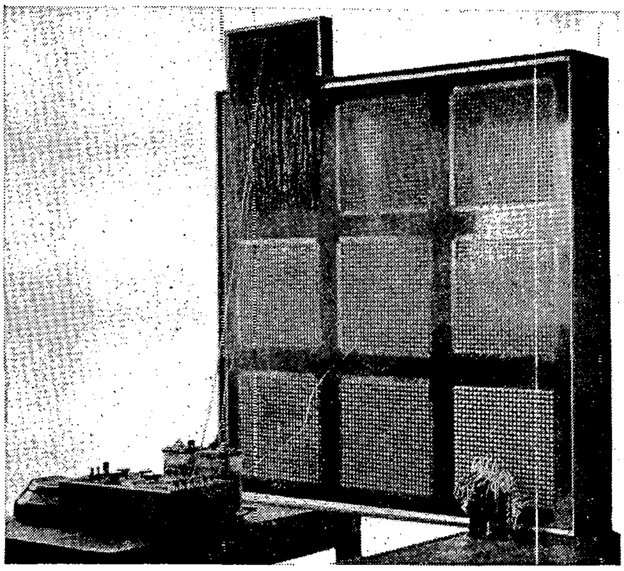

Fig. 1. Potential analyser set up for an experiment

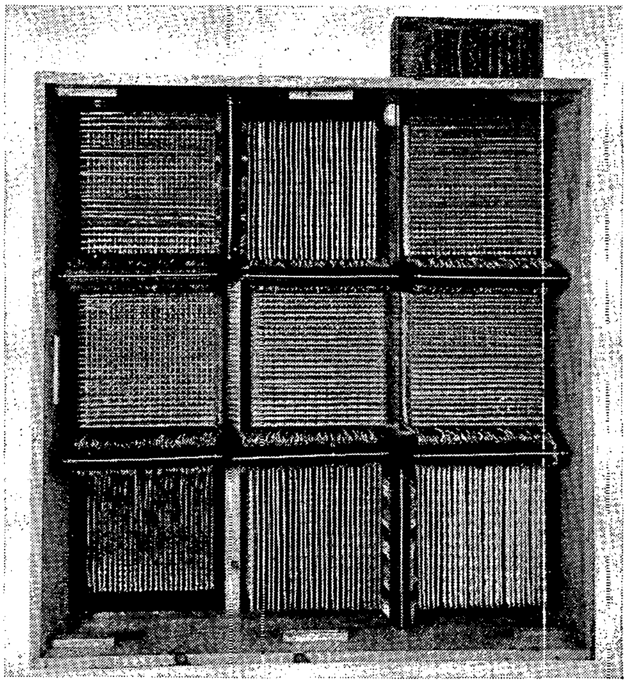

Fig. 2. Rear view of instrument

the corresponding sockets on the tier on either side through a resistor of value identical to that of the unit resistors. The inter-tier resistors were made from woven resistance ribbon, but in this instance separate units were used, the units being mounted in a moulded plastic casing.

The various tiers were connected to the inter-tier resistors by means of harnesses of colour coded leads. Sockets and resistance elements were not assembled on the master tier, but post office type terminals were used instead, these terminals being harnessed to the inter-tier resistors in the normal manner. Resistors, depending on the nature of the particular experiment in hand, were attached to the terminals of the master tier as required. The method of mounting and selecting these resistors will be described later. The resistors on the right-hand side and bottom edges of each tier were doubled in value, while the inter-tier resistors connecting the bottom right-hand corners of each tier were quadrupled in value, thus providing "selvedges" for problems involving a field of single or double symmetry. The reason for using the doubled resistors is that the net can be considered to be slit at the plane of symmetry. When resistance elements are added to the master tier, which is a plane of symmetry, they are also doubled in value. Fig. 2 shows a view taken from the rear of the instrument.

CIRCUIT TESTING

During the construction of the analyser the resistance of each element was checked to ensure that all the units were within a ± 1% resistance tolerance and during the assembly of the instrument each unit was checked for continuity immediately it was installed. When the final assembly had been completed an overall check was made by applying a potential of 1 V across opposite faces of the analyser and then measuring the voltages at each node. This procedure was carried out for each of the three principal axes. In every case the measured potential at each point was within one millivolt of the correct theoretical value.

EXPERIMENTAL PROCEDURE

The first series of experiments were concerned with potential flow, without circulation, around a circular lamina and various plan forms. As with vortex sheet theory the wings were assumed to be infinitely thin. Wing incidence presents no difficulty; as the field of flow at zero incidence is known the flow conditions for any incidence can be immediately calculated providing the flow normal to the surface is determined.

Similar procedures were used for each experiment. It will be remembered that the master tier on which the model is to be set up has no tier resistors; during the setting up procedure these were provided over the area of the model and as this tier is a plane of symmetry the elements used had double the resistance of the corresponding standard mesh resistors. The plan form was set up on the master tier by connecting resistors to the appropriate terminals. The remainder of the tier was short circuited with a heavy copper wire. In cases where the wing possessed two axes of symmetry in plan form, it was possible to set it up on the master tier so that the axes of symmetry coincided with the mutually perpendicular selvedges of the tier. In cases where only one axis of symmetry existed, one selvedge only could be used. The outer ends of the inter tier resistors placed above the first tier were inter-connected and a potential of one volt was maintained between this point and the short circuited portion of the master tier. The selection of a model size required some judgment, the larger the model the more points on its surface would be available for measurement but, on the other hand, the proximity of the boundary would cause some channel restraint.

A voltage of 1 V was applied to the analyser and the board was scanned by plugging in a probe from socket to socket, the potentials being measured by means of a D.72 A type potentiometer by Muirhead Ltd. This potentiometer is capable of reading accurately to 1 mV and therefore all readings were taken to the nearest millivolt. The electrical circuit which was used for the experiments is shown in Fig. 3. The time taken to set up the apparatus and perform various experiments are given in the following table. One semi-skilled person was employed throughout with the assistance of an unskilled person during the reading and recording stage.

Experiment	*Setting up time* (h)	*Reading and recording* *semi-skilled* (h)	*un-skilled* (h)
Rectangular wing	4	24	24
Delta wing	8	32	32
Swept back wing	8	28	28

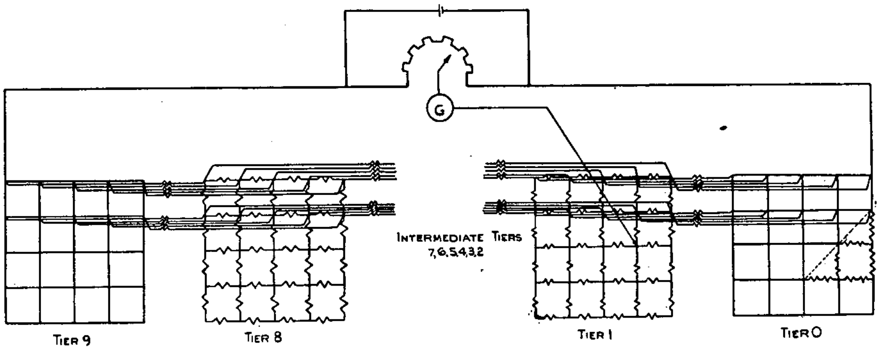

Fig. 3. Electrical circuit for analyser experiments

Three dimensional potential analyser

	6	7	8	9	10	11	12	13	14	15	16	17	18	19
M														
N		0												
O		0	0											
P		0	066	0 0										
Q		0	106	−4 102	−2 0									
R		0	134	−1 164	+1 125	−1 0								
S		0	155	+1 206	+2 199	−7 142	+4 0							
T		0	171	+3 236	−2 250	0 225	−2 153	+1 0						
U		0	182	−4 259	−1 286	−3 281	+4 242	0 160	−1 0					
V		0	192	0 277	0 313	−3 319	−3 300	+3 251	−4 163	−3 0				
W		0	199	0 290	0 333	0 347	0 339	+2 309	+1 254	0 163	+5 0			
X		0	204	−1 299	+2 346	−1 365	−3 364	−2 345	+3 307	+1 247	−1 154	−3 0		
Y		0	207	0 304	0 354	−1 376	−2 379	+1 365	+1 335	−4 291	+6 226	−3 126	−2 0	
Z		0	208	0 306	+1 357	+2 380	+1 384	+2 372	+3 345	+2 304	−1 248	−2 176	+2 086	−2 0

Fig. 4. Three dimensional potential analyser

Problem. Flow normal to flat plate.
Tier 1.

Model size. Delta 12 mesh units semi-span. 12 mesh units root chord uniform voltage of 1·000 at tier 9.

Three dimensional potential analyser

	6	7	8	9	10	11	12	13	14	15	16	17	18	19	
M	113	114	114	114	114	114	113	113							
N	115	116	+2 117	+3 116	−4 116	0 115	115	114	114	113	113	112	112	112	
O	116	119	0 123	−1 122	0 120	−1 118	−2 117	0 116	115	114	113	113	112	112	
P	119	−2 126	−2 145	+3 136	−1 129	0 124	−1 121	+1 118	−2 116	−4 115	114	113	113	113	
Q	123	−1 136	+6 169	+3 172	+1 149	+2 136	+2 128	0 123	0 120	+3 117	−3 116	114	113	114	
R	127	0 144	+3 190	−2 208	−1 194	−2 159	−3 141	−2 131	0 125	+1 121	+1 118	116	115	114	
S	131	+3 151	−3 209	0 240	+2 239	−1 212	−1 168	+1 146	+3 133	−3 126	−1 122	+4 118	116	115	
T	134	−1 159	+6 225	+2 266	+1 277	−3 263	+1 225	−1 174	0 149	+3 135	+2 126	−4 121	−2 118	117	
U	137	+2 164	+2 237	−1 287	+1 308	−2 305	0 279	−2 234	+1 178	+2 150	+1 135	+2 126	−1 121	0 118	
V	139	+2 168	0 247	0 304	+3 333	+3 338	−1 323	−1 289	0 238	+2 178	0 149	+1 134	+3 125	0 120	0
W	140	−2 171	0 254	−3 316	+1 351	+2 353	0 356	−1 332	+1 291	−2 236	+1 174	−6 146	+2 131	+1 123	+2
X	141	−1 173	−3 260	+2 324	−3 363	−1 380	0 379	+2 361	−5 330	+1 284	−2 227	0 168	+3 140	+2 126	−3
Y	142	−2 175	0 263	0 329	−4 371	+4 390	0 392	−1 379	−1 353	0 314	−4 265	0 208	+2 153	−1 131	+2
Z	143	+3 176	+2 264	−1 331	−1 373	1− 393	−2 396	−3 385	−1 361	0 325	+2 279	+4 224	−6 171	+1 135	+4

Fig. 5. Three dimensional potential analyser

Problem. Flow normal to flat plate.
Tier O.

Model size. Delta 12 mesh units semi-span 12 mesh units root chord uniform voltage at 1·000 at tier 9.

RESULTS OF EXPERIMENTS

The presentation and discussion of the results of the various experiments is outside the scope of the present paper but, as examples of the order of accuracy which has been achieved, the values of some of the potentials which were measured on two tiers during one of the experiments are shown in Figs. 4 and 5. The residuals, which have been calculated by the relaxation process from the experimental readings, are also entered on the figures and it will be seen that they are very small; no appreciable improvement could be obtained by the application of the relaxation process to these results.

ACKNOWLEDGMENTS

The potential analyser was designed and constructed for the Ministry of Supply by Boulton Paul Aircraft Ltd., to whom the author wishes to express his thanks for permission to publish this paper; his thanks are also due to Mr. B. F. Clark and Mr. D. M. Bruce for their assistance in the construction of the apparatus and the carrying out of the experiments.

REFERENCES

(1) Southwell, R. V. *Relaxation Methods in Theoretical Physics* (London: Oxford University Press, 1946).
(2) Relf, E. F. *An Electrical Method of Tracing Stream Lines for the Two-Dimensional Motion of a Perfect Fluid.* R. and M. No. 905 (1924).
(3) Taylor, G. I., and Sharman, C. F. *A Mechanical Method for Solving Problems of Flow in Compressible Fluids.* R. and M., No. 1195 (1928).
(4) Kron, G. *J. Aero. Sci.*, **12**, No. 2, p. 221 (1945).
(5) Malavard, L. *J. Roy. Aero Soc.*, **51**, No. 441, p. 739 (1947).
(6) Redshaw, S. C. *Proc. Instn Mech. Engrs*, **159**, p. 55 (1948).

The dielectric behaviour of some types of human tissues at microwave frequencies

By H. F. Cook, B.Sc., Ph.D., A.M.I.E.E., F.Inst.P., Department of Physics Applied to Medicine, The Middlesex Hospital Medical School, London

[*Paper first received* 24 *May*, 1951, *and in final form* 18 *June*, 1951]

The dielectric properties of four types of human tissues have been investigated by a coaxial line method at frequencies corresponding to free space wavelengths in the range 6 to 17 cm. The results have been examined in relation to the Debye dispersion equations and it has been found that the dielectric behaviour of some types of tissues can be described approximately by them if an additional term for ionic conductivity is included. The results have been further discussed with reference to ion and protein hydration and to the ionic conductivities of the intracellular and extracellular fluids.

The object of the measurements to be described was to obtain average propagation constants at microwave frequencies for different types of tissues to aid in the study of the transmission and absorption of centimetre waves in the human body. Several workers have described experiments designed to determine the dielectric properties of animal tissues over a wide wavelength range. The use of condenser field therapy at frequencies corresponding to free-space wavelengths of 3, 6 and 12 m stimulated workers to study particularly tissue dielectric behaviour at these wavelengths. Rajewsky(1) and his collaborators made notable contributions, as also did Osswald.(2) Of interest also are the very high dielectric constants (of the order of 10 000) obtained at much lower frequencies by Iwase(3) using rabbits' tissues. This author reports results from 10^6 cm wavelength (3×10^4 c/s) down to 10^2 cm and discusses briefly the dispersion shown.

At microwave frequencies, the only results on human tissues known to the author are those of England and Sharples,(4) and England.(5) The present work was designed to overlap that of England and to extend the wavelength range used in his investigations to wavelengths longer than 10 cm. Only four types of tissue have so far been investigated, but further work on others is in progress.

EXPERIMENTAL

Method and apparatus.—The method adopted was that described by Roberts and von Hippel.(6) In this method the specimen fills a short length of a waveguide or coaxial line and is terminated by a short circuit. Measurements on a standing wave set up in the guide or line section preceding the specimen then enable the complex dielectric constant, $\epsilon' - j\epsilon''$, to be evaluated.

Signals of wavelengths from 6·5 cm to 17 cm were available, and, to enable measurements to be made on a single specimen over this wavelength range, coaxial line apparatus was employed. This also had the advantage over waveguide apparatus that the specimens required were of much smaller cross-section and bulk.

Normally, standing wave measurements are carried out in an air-filled slotted section of line. For the measurements on bone samples such a procedure was adopted, the apparatus being that used in a previous investigation.(7) In the case of soft tissue specimens a Distrene-filled, slotted, coaxial line was used (Fig. 1). The design was such as to ensure plane specimen interfaces both at the Distrene boundary and at the short-circuiting plunger, with a micrometer method of measuring the rather small (a few millimetres) specimen thicknesses which have to be employed with materials of such high dielectric constant and loss. The correct amount of compression to employ to obtain specimens completely filling the space between the Distrene and the plunger, without damage to the tissues, was found to be easily determined from the "feel" of the lock-nut.

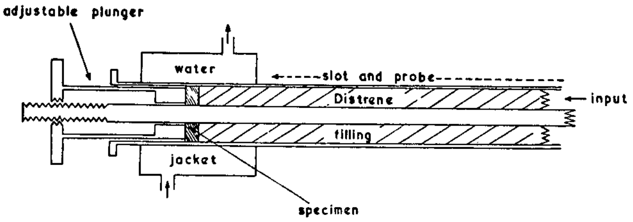

Fig. 1. Diagram (not to scale) of coaxial line apparatus used for measurements on soft tissues

The temperature of the specimens was maintained at 37 ± 0·2° C throughout the experiments by means of a thermostat flow system.

Measurements on the standing wave in the Distrene were made by means of a tuned probe incorporating a rectifying crystal. The wire of the probe moved in an air-filled slot in the Distrene 0·5 mm wide and 1 mm deep. The rectified current was measured by use of a sensitive reflecting galvanometer. Calibration of the detection system was made by measurements on a full standing wave in an air-filled coaxial line. On all occasions the galvanometer deflexions were found to be proportional to the square of the signal strength except at deflexions approaching the maximum. Care was taken in the measurements on the Distrene-filled line that deflexions did not exceed that at which the square law broke down, this square law then being assumed in all the work.

The probe distance from the Distrene interface was measured by a vernier sliding against a steel rule. The fixed distance between the interface and the probe when at the zero of the scale was measured as accurately as possible.

Measurements at different wavelengths on the standing wave in the Distrene with no specimen, and the plunger in contact with the Distrene interface, were made during each series of measurements on tissue specimens. The minima were always equally spaced, showing that the dielectric filling was uniform. The position of the minima obtained at the different wavelengths, in conjunction with the wavelengths measured in Distrene, gave estimates, agreeing within 0·1%, of the prob-interface distance when the scale reading was zero. The mean estimate was in excellent agreement with the value of this distance measured by sliding calipers.

By comparison of the wavelengths measured in the Distrene line and those in an air-filled line wavemeter the dielectric constant of the Distrene was calculated to be 2·50 ± 0·01.

The standing wave ratio in the Distrene line with no specimen was 0·015. The minimum readings at different positions were nearly equal, showing that the dielectric loss in the Distrene had a negligible effect. The loss of power causing this non-zero standing wave ratio was, therefore, considered to occur at the plunger. However, since high loss materials were to be measured this loss was neglected.

Computation of the dielectric constant and loss of specimens from the standing wave measurements was made by use of the relations and method given by Roberts and von Hippel.(6) In the case of the Distrene-filled line, the constants so calculated were with reference to those of Distrene. Hence a multiplying factor of 2·50 was used to refer the constants to that of air.

Experimental results.—The dielectric properties of skin, fat, muscle and bone are the main interest when the propagation of microwaves in the human body is considered. Accordingly, fresh specimens of these types of tissue were obtained from the operating theatre and measurements made as quickly as possible after excision. The measurements were normally completed within three hours from the time of excision.

The results of the measurements are presented in Tables 1 and 2.

It is possible that errors as large as ± 10% may occur in determinations of ϵ'' (the loss of power at the plunger has been neglected). Owing to the many factors contributing to errors in the measurement using the Roberts and von Hippel method it is very difficult to calculate percentage errors for each tissue specimen. It is unlikely that the values of ϵ' given in the tables are in error to greater than ± 3%.

DISCUSSION

(*a*) *Wavelength dependence of the dielectric constants*

As expected there is a spread in the measured values of the dielectric constants of each type of tissue, depending on the anatomical site and probably also on the condition of the patient from whom the tissues were removed. It is not proposed to enter into detailed discussion on the reasons for these differences. Of more immediate interest is the dependence on wavelength of the average dielectric constants of the different types of tissues.

It has already been shown(8) that the dielectric constant at microwave frequencies of whole human blood depends on frequency according to the equations

$$\epsilon' = \frac{\epsilon^* - \epsilon_\infty}{1 + (\omega\tau)^2} + \epsilon_\infty = \frac{\epsilon^* - \epsilon_\infty}{1 + (\lambda_s/\lambda)^2} + \epsilon_\infty$$

$$\epsilon'' = \frac{\epsilon^* - \epsilon_\infty}{1 + (\omega\tau)^2} \cdot \omega\tau + (3{\cdot}6 \times 10^{12})\frac{\pi\sigma}{\omega}$$

$$= \frac{\epsilon^* - \epsilon_\infty}{1 + (\lambda_s/\lambda)^2} \cdot \frac{\lambda_s}{\lambda} + 60\,\lambda\sigma$$

Table 1. *The dielectric constants of skin and muscle at 37° C*

Type of tissue	Specimen from	Wavelength (cm) 16·85 ε'	16·85 ε''	10·07 ε'	10·07 ε''	8·36 ε'	8·36 ε''	6·48 ε'	6·48 ε''
Skin	(*a*) Near faecal fistula	51·5	20·9	51·1	15·2	48·5	13·6	46·1	16·1
	(*b*) Breast	39·7	18·0	40·0	12·3	—	—	38·8	13·4
	(*c*) Instep (sole)	—	—	42·4	13·1	40·0	12·0	39·7	12·5
Muscle	(*a*) Soleus	51·2	24·0	51·0	18·0	48·5	17·5	47·0	20·2
	(*b*) Pectoralis major	50·1	23·3	50·0	17·1	48·0	14·4	46·5	16·3
	(*c*) Pectoralis major	51·5	20·7	52·0	18·9	—	—	48·5	19·5

Table 2. *The dielectric constants of fatty tissue and bone at 37° C*

Type of tissue	Specimen from	Wavelength (cm) 16·85 ε'	16·85 ε''	10·07 ε'	10·07 ε''	8·36 ε'	8·36 ε''	6·48 ε'	6·48 ε''
Fatty tissues	(*a*) Breast	4·2	1·14	3·94	0·87	4·10	0·77	4·06	0·76
	(*b*) Anterior abdominal wall	—	—	4·92	1·46	4·20	1·0	—	—
	(*c*) Near faecal fistula (includes aerolar tissue)	7·24	2·25	7·00	1·75	6·92	1·57	5·75	1·87
	(*d*) Sole of foot	11·1	2·97	11·6	2·25	10·8	1·02	7·74	0·89
	(*e*) Breast (treated by X-rays. Includes fibrous tissue)	16·1	4·53	14·7	3·95	13·5	3·38	8·70	2·40
Bone	(*a*) Anterior medio surface of mid-shaft of tibia	8·4	1·5	8·35	1·32	8·30	1·29	7·83	1·30

where ϵ^* and ϵ_∞ are the values ϵ' approaches on the low and high frequency sides of a dispersion region due to water relaxation,

$\omega = 2\pi \times$ frequency (c/s); $\lambda =$ wavelength (cm)

τ is a single time of relaxation for "free-water" (sec)

λ_s is a "relaxation wavelength" $= (1{\cdot}885 \times 10^{11})\tau$ (cm)

and σ is an ionic conductivity assumed independent of frequency (ohm^{-1} cm^{-1}).

These are the well-known Debye equations containing an additional conductivity term. It was thought of interest to examine whether the present results on skin, muscle, etc., would satisfy these equations approximately.

Skin.—The results for specimens (*b*) and (*c*) show that skin from these sites is similar in dielectric behaviour, whilst that from the site near the faecal fistula gives higher dielectric constants. England obtained the dielectric constants of breast and leg skin at three wavelengths. He reported average values of $43{\cdot}5 - j\,16{\cdot}5$, $35{\cdot}5 - j\,16$ and $23 - j\,13$ at wavelengths of 10, 3·2 and 1·27 cm respectively. His result at 10 cm wavelength is in reasonable agreement with those for specimens (*b*) and (*c*).

Analysis of both England's and the present results then shows that the dielectric behaviour of this type of skin in the microwave region is mainly governed by the relaxation of "free" water and by ionic conductivity. (Effects of inhomogeneity on dispersion of ϵ', as in the case of blood, can be assumed to be negligible at microwave frequencies.) Reasonable agreement (see Fig. 2) between the experimental results and those calculated from the above equations is obtained if, in the latter, the following values are used:

$$\epsilon^* = 42 \qquad \tau = 0{\cdot}69 \times 10^{-11}\ \text{sec}$$
$$\epsilon_\infty = 4 \qquad \sigma = 0{\cdot}014\ \text{ohm}^{-1}\ \text{cm}^{-1}$$

The skin from near the faecal fistula can be regarded as abnormal. The results are approximately consistent with:

$$\epsilon^* = 51 \qquad \tau = 0{\cdot}85 \times 10^{-11}\ \text{sec}$$
$$\epsilon_\infty = 4 \qquad \sigma = 0{\cdot}014\ \text{ohm}^{-1}\ \text{cm}^{-1}$$

The absence of comparable results at shorter wavelengths makes the derivation of these figures much more approximate than in the previous case, though ϵ^* is more certain.

The increase in ϵ^* and τ over the values obtained for the other skin specimens may be attributed to pathological change. The higher ϵ^* may be due either to a higher total water content or to a change in the proportion of the water which is bound to ions or proteins.

It should be noted that the relaxation time of the water in tissues need not necessarily be equal to that of pure water at the same temperature ($0{\cdot}63 \times 10^{-11}$ sec at 37° C). While inorganic ions in aqueous solution decrease the water relaxation time,(9) it has recently been found(10, 11) that hydrogen bonding between water molecules and the active groups of other types of molecule causes an increase in the relaxation time. This latter effect appears to predominate in the case of tissue water, and its magnitude to depend on the type of tissue.

Muscle.—The three specimens measured give results showing little difference in their dielectric behaviour. Following the same procedure as in the case of skin the results agree approximately (Fig. 2) with values calculated using:

$$\epsilon^* = 51 \qquad \tau = 0{\cdot}8 \times 10^{-11}\ \text{sec}$$
$$\epsilon_\infty = 4 \qquad \sigma = 0{\cdot}018\ \text{ohm}^{-1}\ \text{cm}^{-1}$$

England has no comparable results at shorter wavelengths and the absence of these makes the values of τ and σ very approximate.

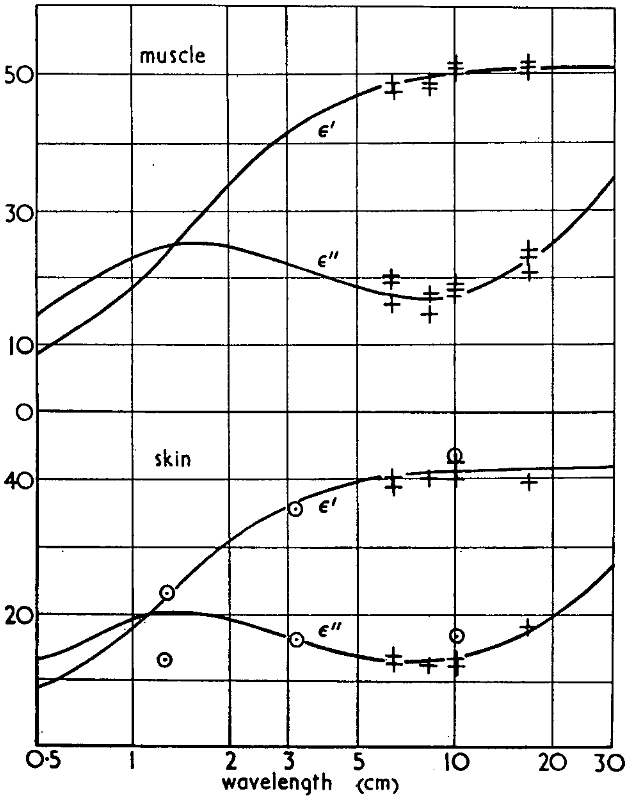

Fig. 2. Variation with wavelength of the dielectric constant (37° C) of skin and muscle tissues

Full line — calculated from Debye equations.
⊙ — experimental results of England.
× — present experimental results.

Fatty tissue.—The results on different specimens of fatty tissue show that their dielectric behaviour is very dependent on the amounts of other types of tissue present. Specimen (*a*) is the nearest approach to pure human fat and the dielectric properties of this show little change in the wavelength range covered.

In the course of other investigations the author measured the dielectric constant of mixed stearins (body fat constituents) at 37° C and at a wavelength of 8·20 cm, giving a result of $2\cdot46 - j\,0\cdot03$. It is reasonable to assume that palmitin and olein (also present in human fat) have similar constants. Comparison, then, with the results for specimen (*a*) indicate that its higher dielectric constant and loss are due to the presence of water and ions. The concentrations of these in specimen (*a*) must be much lower than those in skin and muscle. The other specimens give results consistent with increasing water contents due to increasing proportions of other types of tissue. It is noticeable that the fibrosis caused by X-ray treatment produces a marked effect on the dielectric constant of breast fat.

Specimens of fatty tissue investigated by England have given average dielectric constants of $6\cdot9 - j\,1\cdot6$, $4\cdot5 - j\,0\cdot95$ and $3\cdot4 - j\,1\cdot1$ at wavelengths of 10, 3·2 and 1·27 cm respectively. They would, therefore, appear to behave electrically in a manner approximately corresponding to specimen (*c*) of the present series of fatty specimens. The dispersion cannot be explained as simply as in the case of skin and muscle. The latter types of tissues display dielectric dispersion approximately in the manner of homogeneous materials at microwave frequencies. This can be attributed to the possibility that the dielectric constants (operative at these frequencies) of the extra-, inter- and intracellular fluids are not very different.

Fatty tissue is more heterogeneous at microwave frequencies since the cells containing most of the fat have a low dielectric constant and are dispersed in a medium of much higher dielectric constant. So dispersion in such a material would not be expected to follow, even approximately, that calculated from simple water relaxation alone.

Bone.—The results for the single specimen used in the present work are in fair agreement with the results of England. He obtained, for a specimen taken from the femur, dielectric constants of $7\cdot6 - j\,1\cdot45$ and $6\cdot3 - j\,1\cdot1$ at wavelengths of 3·2 and 1·27 cm respectively. Thus dispersion of ϵ' from 8·4 to 6·3 occurs between wavelengths of 16·85 cm and 1·27 cm. This corresponds approximately to a Debye dispersion with a single relaxation time of $0\cdot7 \times 10^{-11}$ sec. The values of ϵ'', however, do not fit in with this type of dispersion spectrum, with an additional contribution from ionic conductivity. So, as in the case of fatty tissue, the dispersion is probably influenced by inhomogeneity and analysis becomes fraught with difficulties.

(*b*) *Variation of absorption and reflexion coefficients with wavelength*

Calculations of microwave propagation in the human body (to be described elsewhere) have been facilitated by the derivation of the absorption coefficient of various types of tissues at different wavelengths and of the reflexion coefficients of the tissue interfaces (e.g. skin-fat, fat-muscle).

Fig. 3 shows the way in which the signal strength attenuation constant (absorption coefficient) varies with wavelength. The curves for skin and muscle have been calculated from the constants given in the previous section. It has been assumed that the only absorption processes present in the wavelength range 0·5 cm to 30 cm are those of ionic conduction and water relaxation. The curve for fat relates to specimen (*c*) of Table 2, which may be taken as representative of average fatty tissues. This curve, and that for bone, have been drawn through points calculated from the experimental results in Table 2.

Points of interest when the therapeutic use of microwaves is contemplated are that the absorption changes slowly with wavelength from 30 cm down to the region of 10 cm, and that the ratio of absorption coefficients of any two types of tissues remains relatively constant over a greater wavelength range. It is noteworthy that the skin absorption coefficient for microwaves of 1·25 cm

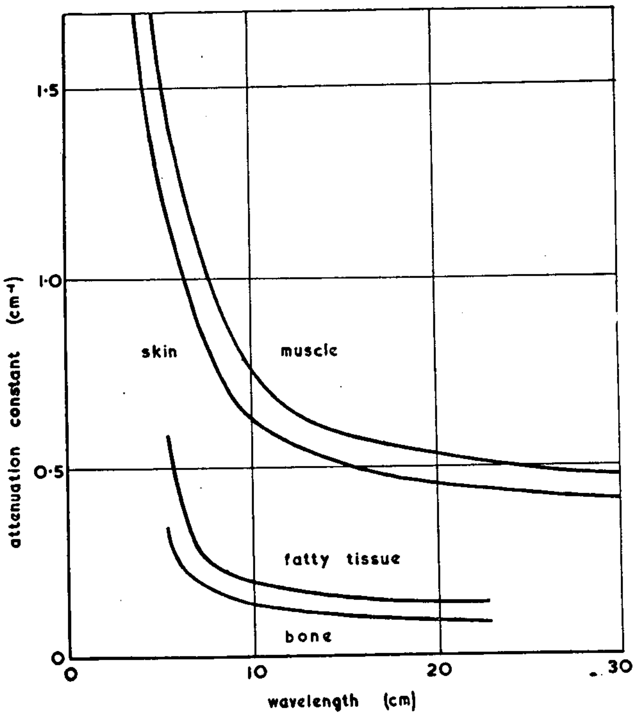

Fig. 3. Variation with wavelength of the attenuation constant of different tissues. (Energy absorption coefficient = 2 × attenuation constant)

wavelength is approximately equal to that for the infra-red radiation from a conventional therapeutic heat lamp.

The reflexion coefficient, $r'e^{jr''}$, of a fatty tissue-muscle interface is given in Table 3.

Table 3. *Reflexion coefficient of fat-muscle interface*

λ	r'	r''
6·5 cm	0·49	0·997 π
8·4 cm	0·47	0·971 π
10·0 cm	0·46	0·987 π
17·0 cm	0·46	0·984 π

The small dependence on wavelength also extends to other tissue interfaces (such as skin-fat, muscle-bone). The coefficients of these interfaces would not be very different from those in Table 3 (if due allowance is made for a change of sign).

(*c*) *The dependence of* ϵ^* *on free-water content and hydration*

The work on human blood[(8)] enabled an estimate of haemoglobin hydration to be made from a comparison of ϵ^* of blood with the corresponding constant for pure water. The theory of Fricke[(12)] for inhomogeneous dielectrics was applied. In the case of skin and muscle insufficient information regarding extracellular volume, cell shape, etc., is available for this theory to be used to obtain a worthwhile estimate of average protein hydration.

However, it can be shown that the different values of ϵ^* for skin and muscle are in accord with their different water, ion and protein concentrations if it is assumed that the dielectric constant is given by a simple volume proportion relation such as that used by Iwase.[(3)] It is thus assumed that the dielectric behaviour of tissues corresponds to a homogeneous dispersion of their constituents.

The chemical composition of human muscle and skin has been published by many workers. The results of Mitchell and others[(13)] have been used here. Taking average protein hydration in these tissues as 0·40 gm per gm,* the static dielectric constant of water at 37° C as 74·1, the depression of this due to ions as given by Hasted and others,[(9)] and assuming that the dielectric constant of bound water, protein, fatty compounds, etc., is 2·0, it can then be calculated that the values of ϵ^* for average skin and muscle at 37° C are 43·7 and 53·8. These are in fair agreement with the experimental values of 42 and 51.

Owing to the lower water contents of fatty tissue and bone, calculations of their dielectric constants from simple volume considerations are of doubtful value and have not been carried out.

(*d*) *Ionic conductivity of skin and muscle*

The electrical conductivity of the tissues of the forearm was measured by Burger and van Milaan[(14)] using direct current. They obtained a conductivity of about 0·004 $\text{ohm}^{-1}\,\text{cm}^{-1}$. It can be assumed that the currents used in their experiments were set up mainly in the extra-cellular fluids (blood plasma and interstitial fluid) of the skin and muscle tissues of the forearm, the membrane reactances of the cells being assumed infinite at zero frequency.

In the present case of microwave frequencies the operative ionic conductivity in skin and muscle is 0·014 and 0·018 $\text{ohm}^{-1}\,\text{cm}^{-1}$, much higher than the zero frequency figure. This increase is due to membrane reactances becoming negligible at microwave frequencies and allowing the intracellular fluid to contribute to the ionic conductivity.

Taking the extracellular volume of skin and muscle tissues as 27%, and applying Fricke's theory[(12)] (using a cell form factor of 2) to the d.c. conductivity of these tissues, it can then be calculated that the conductivity of the extracellular fluid is 0·02 $\text{ohm}^{-1}\,\text{cm}^{-1}$. The micro-wave conductivities are lower than this, indicating that the ionic conductivity of the intracellular fluids is lower than that of the extracellular liquid. A similar result was found for whole blood.[(8)] The conductivity differences between interstitial fluid, blood plasma, and intracellular fluid are related to the different protein concentrations in these liquids, as well as to differences in their ionic concentrations.

---

* This figure is approximately double the hydration which might be estimated from dielectric measurements on skin and muscle proteins if allowance is made for inhomogeneity. When using a dielectric constant relation based on simple volume proportions, the doubling of the hydration factor compensates roughly for the neglect of inhomogeneity.

CONCLUSIONS

The investigation shows that the dielectric behaviour at microwave frequencies of skin and muscle tissues can be approximately described in terms of the Debye dispersion equations with a single relaxation time, if additional dielectric loss due to ionic conductivity is allowed for. It is likely that other tissues in which the electrical behaviour of the intra- and extracellular phases is not too dissimilar would behave in the same way. However, in tissues such as fat and bone, where the phases have large differences in dielectric constant at microwave frequencies, the dispersion is not so simply described.

Reasonable explanations of the dielectric constants and ionic conductivities operative in the microwave region in terms of the hydration of ions and proteins and of differences in conductivity of the extra- and intracellular fluids have been given. It seems possible that microwave measurements on tissues, giving results of higher accuracy than those reported here, could, in conjunction with zero or low frequency conductivity measurements, lead to reasonable estimates of protein hydration and fluid volumes and conductivities.

The propagation constants, which can be derived from the dielectric constants, together with the reflexion coefficients shown in Table 3, have enabled calculations to be made of the field strength and energy distributions in parts of the human body exposed to plane wave radiation. These will be the subject of another paper.

ACKNOWLEDGMENTS

Thanks are due to Dr. A. J. H. Hewer and Mr. G. Rigby-Jones for providing tissue specimens, and to Professor J. E. Roberts for his interest in the work.

REFERENCES

(1) RAJEWSKY, B. *Radiology*, **31**, p. 697 (1938).

(2) OSSWALD, K. H. F. *Technik u. Elektroak.*, **49**, p. 40 (1937).

(3) IWASE, Y. *Theory and Application of High Frequency Phenomena*, p. 21 (Hokkaido University, Japan, 1950).

(4) ENGLAND, T. S., and SHARPLES, N. A. *Nature*, **163**, p. 487 (1949).

(5) ENGLAND, T. S. *Nature*, **166**, p. 480 (1950).

(6) ROBERTS, S., and VON HIPPEL, A. *J. Appl. Phys.*, **17**, p. 610 (1946).

(7) COOK, H. F., and BUCHANAN, T. J. *Nature*, **165**, p. 358 (1950).

(8) COOK, H. F. *Nature*, **168**, p. 247 (1951).

(9) HASTED, J. B., RITSON, D. M., and COLLIE, C. H. *J. Chem. Phys.*, **16**, p. 1 (1948).

(10) COOK, H. F. *Trans. Faraday Soc.*, **47**, p. 751 (1951).

(11) HASTED, J. B., HAGGIS, G. H., and HUTTON. *Trans. Faraday Soc.*, **47**, p. 577 (1951); (and private communication).

(12) FRICKE, H. *Phys. Rev.*, **24**, p. 575 (1924).

(13) MITCHELL, H. H., HAMILTON, T. S., STEGGERDA, F. R., and BEAN, H. W. *J. Biol. Chem.*, **158**, p. 625 (1945).

(14) BURGER, H. C., and VAN MILAAN, J. B. *Acta Med. Scand.*, **114**, p. 584 (1943).

The preparation of high melting point metal single crystals and bicrystals with pre-determined crystallographic orientation

By K. V. GOW, M.Sc., and B. CHALMERS, D.Sc., Department of Metallurgical Engineering, University of Toronto

[*Paper received* 7 *May*, 1951]

A method is described for the preparation, in metals of high melting points, of single crystals and bicrystals with predetermined crystallographic orientations. The crystals are grown horizontally in an atmosphere of argon; heating is by graphite rod resistors. The method has been applied to copper and nickel.

The importance of the investigation of metal single crystals has been demonstrated in recent years. However, many properties of a metal in its usual condition are related to the fact that it is an aggregate of many small crystals. The effect which each crystal exerts on the neighbouring crystals has a powerful influence on the properties of the metal. To investigate these effects, it is necessary to study the regions between the crystals—that is, the crystal boundaries. It is more fruitful to study the properties and effects of a single boundary between two crystals than to infer them from specimens containing many crystals and boundaries. A specimen consisting of two crystals of different, but controlled, crystallographic orientation, joined by a single boundary, is called a bicrystal. Fig. 1 illustrates a bicrystal and the single crystal seeds from which it is grown.

Many techniques have been developed for the preparation of metal single crystals. Holden[(1)] gives an extensive list of references with a discussion of the basic methods employed. The Bridgeman method[(2)] of producing large single crystals from the liquid metal in a vertical furnace has been refined by Goetz[(3)] so that the orientation can be controlled by the use of seed crystals. Horizontal growth from a seed crystal has been adapted by Chalmers[(4,5)] to the preparation of bicrystals.

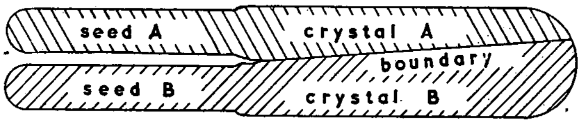

Fig. 1. Diagram of a bicrystal

These are grown from two seed crystals placed in such a position that upon slow solidification of the melt the two crystals will grow in the same direction and be joined by a crystal boundary. The apparatus used by Chalmers for growing bicrystals and single crystal seeds is limited to the metals with low melting points such as tin, lead, zinc and aluminium. This article describes a method which is used for growing single crystals and bicrystals of copper and nickel. Some advantages of this method are:

(*a*) A smooth, thermally-etched and relatively strain-free surface is obtained on the top of the crystal. This eliminates the need for preparing the surface by the usual metallographic techniques prior to investigating such properties as micro-hardness, ferro-magnetic domain structures, etc.

(*b*) The top surface of the crystal may be observed while growth is taking place. The position of the interface between solid and liquid is visible and this simplifies "seeding on" and control of the rate of growth of the crystal.

(*c*) The graphite rod heating elements are inexpensive and easily replaced. They can be in close proximity and directly exposed to the metal.

PRINCIPLE OF THE METHOD

In order to achieve the highest chance of success in growing a crystal, it is necessary that the greatest possible proportion of the heat which leaves the liquid should do so by conduction through the interface and into the solid. This is brought about by maintaining a steep temperature gradient and by allowing the interface to move slowly so that the rate of release of latent heat is slow. The problems encountered in applying these principles to metals with high melting points are: (1) close control of the temperature distribution in the specimen, and (2) the necessity for protecting the specimen from chemical reaction with its surroundings. In the present apparatus, the specimen is heated by means of graphite resistors in close proximity to it. The temperature gradient is maintained by water cooling near the end of the specimen. The interface is caused to move by changing the current through, and hence the temperature of, the resistors; this method avoids the use of moving parts. An atmosphere of argon is maintained round the specimen which is supported in an alumina "boat."

DESCRIPTION OF APPARATUS

The furnace is constructed as shown in Fig. 2. It consists of two parallel, horizontal graphite rod heating elements *A*, the ends of which are clamped to water-cooled copper terminals *B*. Power leads *C* are of $\frac{1}{4}$ in copper tubing which also carries the cooling water to the terminals. The terminals are encased in lead castings *D*, and rest on a water-cooled rack *E* from which they are separated by rubber insulators. The rack is supported in a cantilever position by the end plate *F*. The furnace casing *G* is a 10 in diameter steel cylinder of $\frac{1}{4}$ in wall thickness, water cooled by $\frac{3}{8}$ in copper tubing *H* soldered to it. The casing is mounted on a truck on tracks and, when rolled into operating position (as in Fig. 2), is held against the end plate by two tie-rods *J* and sealed gas tight with a Neoprene gasket *K*. Two glass windows *M* in the top of the casing permit observation of the melt which is necessary particularly during the "seeding on" operation. A Wilson seal *N* in the casing wall, through which a $\frac{1}{8}$ in silica rod *P* is inserted, allows the introduction of mechanical motion such as stirring or skimming the melt. The Wilson seal is designed to allow the rod a lateral motion, the Neoprene gasket in the seal acting as a fulcrum. To form the heating chamber inside the furnace casing, a 1 in thick layer of highly refractory insulating firebrick (not illustrated) is built around the graphite rods. This forms a chamber about $1\frac{1}{2}$ in high, $2\frac{1}{2}$ in wide and 14 in long. The bricks are fitted loosely together and are supported by the water-cooled rack. A slit about $\frac{1}{4}$ in wide and 4 in long is left in the top of the brickwork so that the melt and seed crystals can be observed from the windows. The silica rod is also passed through the slit. Sheet iron radiation shields (not illustrated) at either end of the chamber protect the terminals from direct radiation. Temperatures obtainable in the furnace are limited by the power input available, by the quality, quantity and arrangement about the

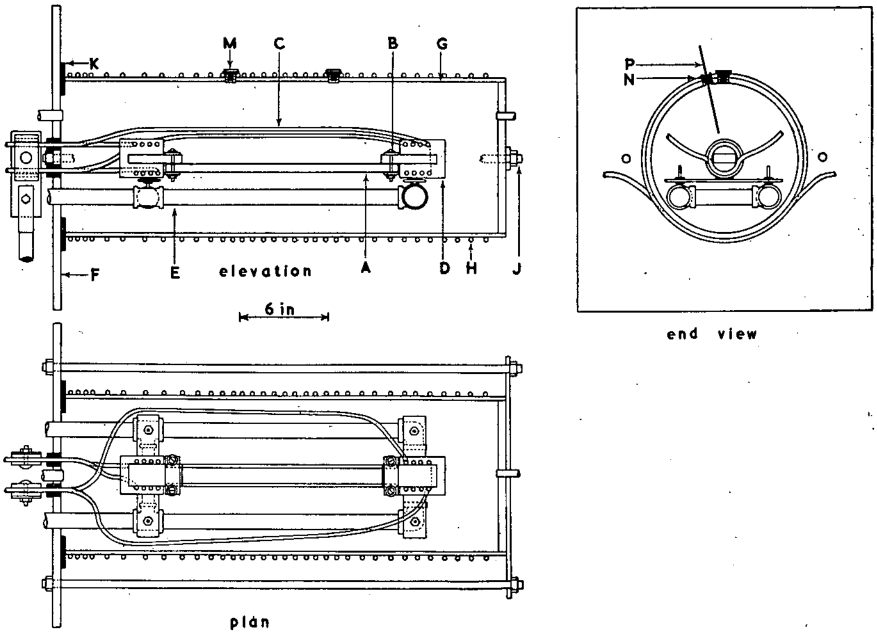

Fig. 2. Diagram of apparatus

elements of the refractory materials used, and by the sublimation temperature of the graphite elements. The maximum temperature used is about 1 600° C which is attained half-way between the terminals. Thus, there are two zones, from the centre of the furnace to either end, in which conditions are satisfactory for the growth of metal single crystals from the melt. Either zone can be used or both simultaneously. The important conditions provided in this way are: (1) a steep temperature gradient of about 1 600° C in 8 in. in the case of nickel, and (2) control of the rate of growth to any desired speed by varying the rate of lowering the power input. The furnace is intended for use with an inert gas atmosphere, argon in this case. It is connected through the end plate to a high vacuum rotary pump for evacuation prior to introducing the argon. The vacuum is measured with a McLeod type gauge connected to the furnace through the casing on one leg of a two-way glass stop-cock, the other leg of which serves as a vacuum release or atmosphere outlet. The atmosphere inlet is through the furnace casing. A small positive pressure of argon is maintained in the furnace during operation. This is indicated by the inflation of a 6 in rubber meteorological balloon connected by a glass tee in the vacuum rubber tubing line from the argon cylinder to the furnace. The pressure is controlled by bleeding argon through the outlet valve during heating or letting argon in during cooling. A static atmosphere is maintained during crystal growth. "Welding grade" argon is used and no purification of the gas is necessary.

Copper single crystals and bicrystals are grown in a graphite boat. The boat is held in cantilever position from one of the water-cooled terminals, since graphite in contact with oxide refractories at these temperatures results in chemical reduction of the oxides. The boats are machined from $\frac{1}{2}$ in thick graphite plates on a milling machine. They provide a trough 8 in × 1 in × $\frac{3}{8}$ in with $\frac{1}{8}$ in walls and bottom. For growing the narrower single crystals, graphite inserts in the trough may be used to reduce its width. Nickel crystals are grown in alumina boats which are open at one end for placing seed crystals. Single crystals are grown in boats 5 in × $\frac{1}{2}$ in wide × $\frac{3}{8}$ in deep and bicrystals in boats 4 in × 1 in wide × $\frac{1}{2}$ in deep. The walls and bottom of the boats are $\frac{1}{16}$ in thick. The alumina boats are supported for their full length on slabs of insulating firebrick. They have a life of three or four melts and fail by warping and cracking. Graphite boats last for many melts.

The power supply is obtained from a 200 kVA, 25 c/s, single phase, step-down transformer with output voltage tapped at 122 V. This feeds two 7 kVA, 230 V, 60 c/s, voltage control Variac transformers connected in parallel to carry a maximum current of 62 A at 122 V. The Variacs feed a 30 kVA, 25 c/s, single phase, 9·5 : 1, step-down transformer. The furnace is connected across the secondary of this transformer. This arrangement permits continuous control of current input to the furnace from 0 to 600 A at 0 to 13 V approximately. The central section of the $\frac{1}{2}$ in diameter, 16 in long, graphite rod heating elements are machined flat along one side for 14 in in a milling machine, so that connected in parallel, their total resistance is about 0·02 Ω when cold. This allows the maximum power input to the furnace of 7 kVA. The current is measured with an ammeter in the Variac secondary circuit.

METHOD OF OPERATION

To grow the initial single crystal, which can thereafter be used as a seed crystal, it is necessary to cause a single nucleus to form and to grow. To do this a $\frac{1}{4}$ in diameter copper rod is soldered to one of the water-cooled terminals. The rod projects into the heating chamber, and embedded in the end of the rod is a $\frac{1}{2}$ in length of $\frac{1}{8}$ in silica rod ground to a point. This serves as a "heat wick." The copper rod is bent so that the pointed silica tip touches the cool end of the pool of liquid metal. This is most easily done by having the boat at an angle of about 1° to the horizontal so that the metal will flow toward the cool end and rest against the silica tip. The action of this "heat wick" is to super-cool as small a volume of the metal as possible so that only one nucleus will form. Formation of this nucleus and growth of a single crystal from it is brought about by slowly lowering the power input to the furnace. In this way the interface between solid and liquid moves toward the centre of the furnace and in so doing the metal is crystallized progressively. The progress of growth may be followed by observing the position of the interface through a window in the furnace casing. Crystals are grown at a rate not exceeding 2 mm/min. By having the heating elements along either side of the boat and a water-cooled terminal at the cold end, ideal heat flow conditions are approached. The copper rod "heat wick" and the seed crystals also serve to promote withdrawal of heat from the cold end while heat flows into the liquid phase.

Single crystals may be grown in any crystallographic direction, but there is a preferred direction of growth which is usually one of the principal axes of the crystal. Thus, if the crystal is grown in a direction in which growth is more difficult, there is more likelihood of "stray" crystals forming. A bicrystal may also be grown with any crystallographic directions, but for nickel, and probably for other high melting point metals, it is necessary that the orientations of the crystals should be symmetrical to within a few degrees about the axis of the boat. This is to cause the boundary to grow parallel to the axis of the boat.(6) If the condition of symmetry is not satisfied, the boundary will grow at an angle to the axis of the specimen, and it may then move back until it is between one of the seed crystals and the rest of the specimen. The much smaller cross-section of the seed crystal then corresponds to a smaller area and, therefore, lower energy of the boundary. The migration of the boundary is rapid at the melting point of nickel.

Instead of a bicrystal, a large single crystal of the same orientation as one of the seed crystals is obtained. As with single crystals, "strays" are more likely to occur when difficult growth directions are used for bicrystals. Slow rates of growth, about 0·5 mm/min, may help to stop stray crystals forming and minimize the formation of striations. Chalmers(6) has analysed the conditions governing the direction of growth of the crystal boundary in bicrystals of tin and lead.

The procedure for growing a crystal is to fill the boat with the metal to be melted. The seed crystals or copper rod heat wick are placed in position. The cool ends of the seed crystals are supported on blocks or layers of sheet of the same metal as the crystal itself. This helps to keep the seeds cool and prevents their melting back too far. The two seed crystals of a bicrystal are separated by a very thin alumina shield for the distance that the seed crystals are to be melted back. The shield is ground to about 0·005 in thick on a fine abrasive wheel. The volume of the shield is reduced in this way so that it will reach the same temperature as the metal and not cause nucleation of unwanted crystals. The shield is prevented from being floated out of position by placing a block of alumina across its thick end. The refractory lining is placed in position and the cooling water is turned on. The furnace is sealed and the chamber evacuated to about 50 μ of mercury. The chamber is then filled with argon so that a slight positive pressure is indicated by the balloon. The power is turned on and the temperature raised rapidly. A nickel charge of 50 to 200 g is melted in about 20 min. As the liquid metal is observed to join on to the seed crystal, the power input is lowered by an amount sufficient to allow about $\frac{1}{4}$ in of the seed to melt. The power is then slowly decreased and the solid-liquid interface moves toward the centre of the furnace. When growth is completed, the furnace may be cooled rapidly so that in about one hour the crystal can be removed. The procedure for growing a bicrystal 3 in long takes about four hours, including the setting up, heating, growing and cooling times.

The seed crystals used for growing a bicrystal should be nearly parallel to each other and in a horizontal plane. This facilitates the "seeding on" operation. Thus, it is necessary to grow seed crystals with the required crystallographic orientation prior to using them for a bicrystal. The orientation of the initial seed crystal is determined from a Laue back-reflexion photograph. The seed crystal is then mounted in the furnace at such an angle that the crystal grown in a horizontal plane by seeding on to it will be of the desired orientation. It may be necessary to go through several stages before the required single crystal is obtained. For example, a nickel seed crystal with the [100] direction as its axis of growth and the (100) plane parallel to the top surface can be grown in a [110] direction with the (100) plane still parallel to the top surface. The geometry of the boat and furnace makes it difficult to do this in one operation with the seed in a horizontal plane at 45° to the required axis of growth. Therefore, the seed is rotated 90° about its long axis and tilted 45° in a vertical plane. The crystal grown from this has a [110] direction of growth and a (110) plane parallel to the surface. The original seed is cut off and the new crystal is rotated 90° about its long axis and another crystal is grown straight from it. This last crystal has a [110] direction of growth and a (100) plane parallel to the top surface.

It is often necessary to cut a crystal and, to avoid straining the crystal, the cutting is done electrolytically. The part of the crystal to be immersed is wrapped in an acid resisting adhesive tape (electroplating tape) except for a $\frac{1}{8}$ in strip around the crystal where it is desired to cut through. The crystal is then suspended vertically in a 10% sulphuric acid-water bath. It is made the anode, and a water-cooled copper tubing coil is used as the cathode. A current of about 10 A cuts through the crystal in a few hours.

ACKNOWLEDGMENTS

The authors wish to express their indebtedness to the National Research Council, Ottawa; the Defence Research Board, Ottawa; and the School of Engineering Research of the University of Toronto, for financial assistance. Their thanks are also due to Dr. L. M. Pidgeon for much helpful advice.

REFERENCES

(1) Holden, A. N. *Trans. Amer. Soc. Metals*, **42**, p. 319 (1950).
(2) Bridgman, P. W. *Proc. Amer. Acad. Arts and Sciences*, **60**, p. 305 (1925).
(3) Goetz, A. *Phys. Rev.*, **35**, p. 193 (1930).
(4) Chalmers, B. *Proc. Roy. Soc. A*, **162**, p. 120 (1937).
(5) Chalmers, B. *Proc. Roy. Soc. A*, **175**, p. 100 (1940).
(6) Chalmers, B. *Proc. Roy. Soc. A*, **196**, p. 64 (1949).

Correspondence

The effect of oxide impurities upon the initiation of arcs

During recent experiments with the electric arc in hydrogen at low gas pressures it was found that the purity of the metal constituting the cathode affected the value of the potential difference at which the arc could be initiated between fixed electrodes. The arrangement was similar to that described by Edels.(1) The impulse necessary to start the arc came from a 2 kV generator and in one set of experiments, with the fixed distance between the tungsten electrodes 3·9 mm and the gas pressure 10^{-3} mm of mercury, the arc struck at 210 V arc supply voltage, the polarity of the impulse discharge voltage being the same as that of the arc voltage. The presence of small traces of oxide, such as calcium oxide, barium oxide, etc., on the cathode, decreased the value of the arc supply voltage at which the arc was initiated to 145 V.

This effect occurred with other metallic electrodes including nickel and aluminium. As pointed out by Edels, the conditions for arc initiation by impulse require that the impulse discharge voltage must be less than that of the arc supply voltage, the inequality being maintained for a time sufficient for the current from the arc source to attain an arc value. The oxide impurities increase the current passing after the initial spark, i.e. the conductivity in the gap between the electrodes is increased and the arc current is built up at a lower arc supply voltage. Llewellyn Jones and Davies⁽²⁾ have shown that a thin oxide film on the cathode can produce enhanced pre-breakdown electron emission. In addition, Salvage⁽³⁾ found that the electric strength of various organic liquids depends upon the electrode metal. Traces of oxides produce marked effects on arc or spark discharges and affect the working of Geiger counters.

F. H. Newman
University College, Exeter.

(1) Edels, H., *Brit. J. Appl. Phys.*, **2**, p. 171 (1951).
(2) Llewellyn Jones, F., and Davies, D. E. *Proc. Phys. Soc. B*, **64**, p. 397 (1951).
(3) Salvage, B. *Proc. Instn Elect. Engrs*, **98**, Part 1, p. 227 (1951).

Magnetostriction storage systems for a high speed digital computer

A continuously variable delay line using the magnetostriction effect in nickel, has recently been described⁽¹⁾ for use with pulses of 1 or 2 μsec duration in a navigational aid system. Delay lines of similar type have been developed in these Laboratories as storage elements for an electronic binary digital computer.

For use in a storage system similar to those incorporating the mercury delay line,⁽²⁾ a 60 μsec delay line consists of a length of about 30 cm of thin tape (nickel or 50% nickel-iron are suitable materials) suitably terminated at each end to suppress reflexions and threaded through a small transmitting coil near one end and a receiving coil near the other end. That portion of the tape within the transmitting coil is magnetized by an adjacent permanent magnet so that a pulse of appropriate shape is launched in the tape when a current pulse is passed through the transmitting coil. A pentode type E.F. 55 coupled to a pulse transformer, is used to drive the transmitting coil and three stages of video amplification are required to produce an output signal of about 30 V. Clock pulses from the computer at 333 000 c/s are gated by this output and the system made regenerative by mixing the resulting output with the signal input to the driving circuit.

The chief advantages of the magnetostrictive delay line store over the mercury delay type may be summarized as follows: (i) greater inherent simplicity and ruggedness; (ii) smaller insertion loss, which is almost independent of the total delay; (iii) the output is easily available at any point along the delay line and may be obtained without interference with the acoustic pulse in the line.

Methods are being developed whereby a long delay line (e.g. 1 msec) may be enclosed in a small space. These methods, apart from purely space-saving considerations, will also facilitate the use of temperature control which may be necessary for longer delay times.

We have also shown that a static storage system can be constructed using the magnetostrictive line. The nature of the output pulse obtained from the receiving coil depends upon the state of magnetization of the tape within it and information can be stored in the tape as remanent magnetization. Thus it is possible to represent the digit "1" by, say, positive remanent magnetization and the digit "0" by zero or negative remanent magnetization. One receiving coil is required for each storage position, the coils being spaced so that the pulse travels from one coil to the next in a time equal to the period between digits. If, for example, the coils are connected in series then when a sampling pulse is transmitted down the line the stored information is reproduced as a series of pulses at the output. The advantages of this system are that the storage is permanent and is not destroyed by the action of reading out the information.

A fuller description of these systems, parts of which form the subject of a patent application, will be published later.

Research Laboratories,
Elliott Brothers (London) Ltd.,
Elstree Way, Boreham Wood,
Hertfordshire.

R. Millership
R. C. Robbins
A. E. De Barr

(1) Bradburd, E. M. *Elect. Commun.*, **28**, p. 46 (1951).
(2) Wilkes, M. V., and Renwick, W. *Electronic Engng*, **20**, p. 208 (1948).

Journal of Scientific Instruments

Contents of the October issue

SPECIAL ARTICLE

British Instrument Industries Exhibition—London, 1951. By M. W. Thring.

ORIGINAL CONTRIBUTIONS

A 35 mm high-speed cinematograph camera. By W. D. Chesterman and D. T. Myers.

A spectrocomparator for the analysis of mixtures using cathode-ray tube presentation of absorption difference specta. By E. F. Daly.

An oil-free gas-tight compressor By G. O. Jones.

A note on the solution and synthesis by inspection of a.c. bridges. By P. B. Fellgett.

Developers for hot-drum processing machines. By A. V. Holden, G. I. P. Levenson and N. Wells.

CORRESPONDENCE

Measurement of wall temperatures—From W. Koch.

Range measurements in nuclear emulsions having a high background—From V. E. Dyke.

Oscilloscope for observing long-duration transients—From E. F. Good and A. E. Ferguson.

The effect of change of angle of incidence on the calibration of infra-red prism spectrometers—From W. Guy and J. H. Towler.

LABORATORY AND WORKSHOP NOTES

Making up very dilute gas mixtures. By D. C. Spanner.

Infra-red absorption cell for volatile liquids. By K. S. Tetlow.

A mechanism for use with polarizing light modulators. By R. W. G. Hunt.

A multi-electrode ring for a vacuum plant. By K. M. Greenland.

THIS JOURNAL is produced monthly by The Institute of Physics, in London. It deals with all branches of applied physics (including theory and technique). All rights reserved. Responsibility for the statements contained herein attaches only to the writers.

EDITORIAL MATTER. Communications concerning editorial matter should be addressed to the Editor, The Institute of Physics, 47 Belgrave Square, London, S.W.1. (*Telephone:* Sloane 9806.) Prospective authors are invited to prepare their scripts in accordance with the *Notes on the Preparation of Contributions*. (Price 2*s*. including postage.)

ADVERTISEMENTS. Communications concerning advertisements should be addressed to the agents, Messrs. Walter Judd Ltd., 47 Gresham Street, London, E.C.2. (*Telephone:* Monarch 7644.)

SUBSCRIPTION RATES. A new volume commences each January, and annual subscriptions will only be accepted for complete volumes of the monthly parts (January–December). The charge is £4 per volume ($11.50 U.S.A.), including index (post paid), payable in advance. Single parts, so far as available, may be purchased at 8*s*. each ($1.15 U.S.A.), post paid, cash with order. Orders should be sent to The Institute of Physics, 47 Belgrave Square, London, S.W.1, or to any Bookseller.

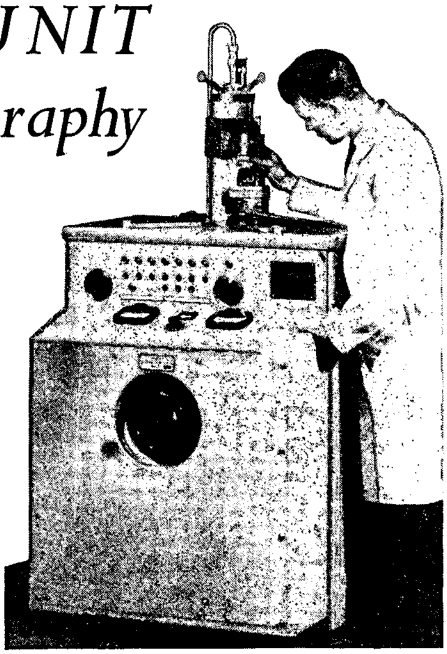

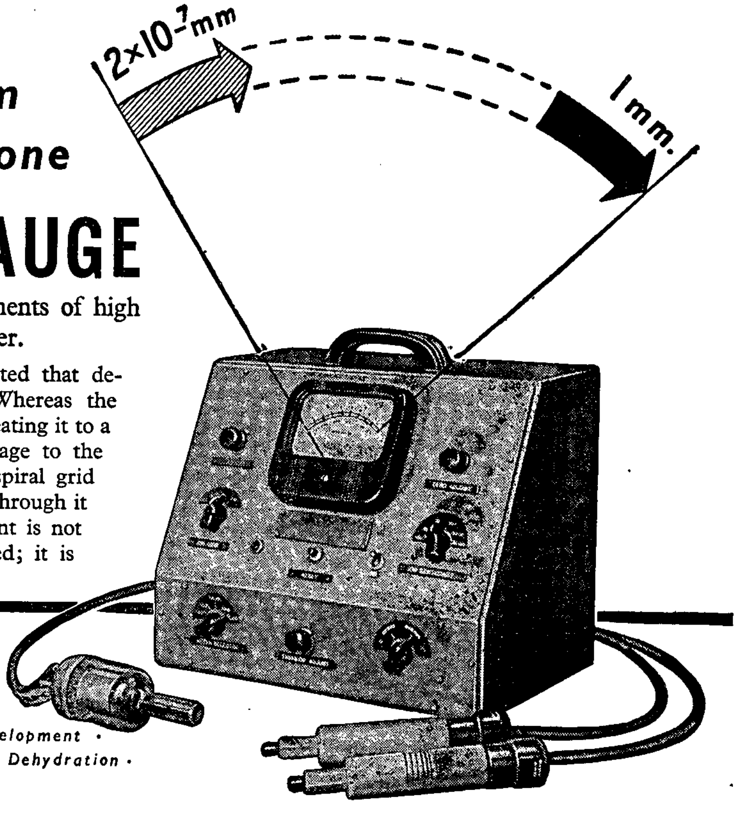
2×10⁻⁷mm
1mm.

The
INSTITUTION OF ELECTRICAL
ENGINEERS

Science Abstracts

SECTION A PHYSICS
SECTION B ELECTRICAL ENGINEERING

A complete reference guide to the world's scientific literature in all aspects of Physics and Electrical Engineering. More than 1 000 abstracts per month, of articles taken from over 600 British and foreign periodicals. Complete Author and Subject Indexes published annually.

Subscription rates obtainable on application to The Secretary,
The Institution of Electrical Engineers, Savoy Place, London, W.C.2.

PHYSICS IN INDUSTRY SERIES
THE MEASUREMENT OF STRESS AND STRAIN IN SOLIDS
Edited by F. A. VICK, O.B.E., Ph.D., F.Inst.P.
Pp. xvi + 114
with 33 illustrations and 8 plates
17s. 6d. (posting and packing 10d. extra). (Available to all grades of The Institute of Physics at 10s. 0d.)
Published by THE INSTITUTE OF PHYSICS
47 Belgrave Square, London, S.W.1

THE BRITISH THOMSON-HOUSTON CO. LTD., RUGBY, Warwickshire, have several vacancies, existing and forthcoming, for electrical engineers and physicists with first- or second-class honours degrees, to expand a group engaged in research and development work on centimetric valves, especially magnetrons. Post-graduate experience of radar, radio and electronic circuits, vacuum techniques etc., is an advantage, although not essential. Applications should be addressed to the Director of the Research Laboratory and should state age, qualifications and experience.

PHYSICS IN INDUSTRY SERIES
THE ACCELERATION OF PARTICLES TO HIGH ENERGIES
Based on a Session arranged by the Electronics Group at The Institute of Physics Convention in May, 1949
10s. 6d. net (postage and packing 10d.) ($1.50 U.S.A.)
Special rate to members of The Institute of Physics of 7s. 6d., including postage
Foreword by
PROFESSOR M. L. E. OLIPHANT, F.R.S.
Papers by
PROFESSOR J. ROTBLAT
MR. F. K. GOWARD
DR. E. S. SHIRE
Discussion edited by
MR. V. J. FRANCIS
Published by
THE INSTITUTE OF PHYSICS
47 Belgrave Square, London, S.W.1

Supplement to

JOURNAL OF SCIENTIFIC INSTRUMENTS

VACUUM PHYSICS

This supplement contains the papers presented at a symposium arranged by the Midland Branch of the Institute of Physics in June 1950.

CONTENTS

Modern vacuum pumps; The vacuum system of the Birmingham proton synchrotron; General principles of leak detection; Recent advances in vacuum coating plant and technique; Melting and sintering of metals in vacua; Application of the mass spectrometer to high vacuum problems; Vacuum pumps for freeze drying; Large scale vacuum dehydration; The design of industrial vacuum systems; A cold-cathode mass spectrometer leak detector; Review of vacuum gauges.

Subscribers to the Journal of Scientific Instruments will receive a paper-bound copy with the October issue of the Journal.

Additional copies bound in boards will be available in October.
PRICE: 15s. 0d. (postage and packing 10d. extra).
U.S.A. $2.25 (including postage and packing).

THE INSTITUTE OF PHYSICS
47, Belgrave Square, London, S.W.1. SLOane 9806

PHYSICS IN INDUSTRY

CREEP OF METALS

By

L. ROTHERHAM, M.Sc., F.Inst.P

A monograph specially commissioned by The Institute of Physics

The contents include

The Characteristics of the
Creep Curve; Crystalline Flow; Metallographic Features of Creep; Grain Boundary, Transient, Steady-state, and Tertiary Creep; and the Development of Creep-resistant Alloys

To be published shortly

Price 15*s.* 0*d.*

(*postage and packing* 10*d.*)

Members of The Institute of Physics are entitled to one copy each for their PERSONAL use at a reduced price if application is made on the special form provided.

THE INSTITUTE OF PHYSICS
47, Belgrave Square, London, S.W.1—SLOane 9806

OPTICAL FILTERS

Barr and Stroud narrow-band filters offer a convenient method of isolating spectrum lines, in flame photometry or the mercury arc, or of filtering white light to obtain any required colour value.

The graph illustrated is a careful reproduction of an actual measurement of a series "A" type (general purpose) filter for use when strictly collimated light is not available.

Barr and Stroud Ltd. produce a wide range of optical filters for many purposes. They include wide and narrow-band colour filters and neutral filters, both uniform and graded.

ENQUIRIES FOR SPECIAL PURPOSES ARE INVITED

BARR & STROUD LTD.

ANNIESLAND,
GLASGOW, W.3

15 Victoria Street,
LONDON, S.W.1

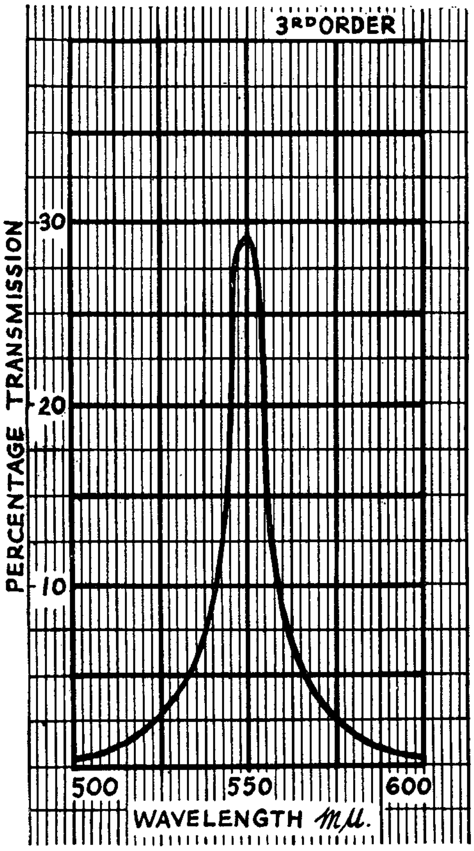

SPECIAL PURPOSE ALLOYS

TELCON THERMOSTATIC BIMETALS

A range of precision bimetals noted for their stability and suitable for all applications involving temperature control, indication or compensation.

TYPE	BIMETAL 140	BIMETAL 400	BIMETAL 15
Composition Low Expansion % Ni	38	42	36
Composition High Expansion % Ni	20	20	100
Deflection Constant per °C. (d)	14.0×10^{-6}	11.0×10^{-6}	9.7×10^{-6}
Resistivity michrohms/cm. cube at 20°C.	75	70	15
Maximum Working Temp. °C.	300	400	200

Our Representative will call, or full technical data will be sent on request

TELCON METALS

TELCON TCM Founded 1864

THE TELEGRAPH CONSTRUCTION & MAINTENANCE CO. LTD.

Head Office: 22 Old Broad St., London, E.C.2. Phone: LONdon Wall 7104
Enquiries to: Telcon Works, Greenwich, S.E.10. Phone: GREenwich 3291

B. H. BLACKWELL, Ltd.

48–51 BROAD STREET,
OXFORD

Specialists in Books for Specialists

We can supply BRITISH, AMERICAN and FOREIGN BOOKS AND PERIODICALS on all aspects and latest developments of THEORETICAL AND APPLIED PHYSICS, LABORATORY PRACTICE, and INDUSTRIAL APPLICATIONS.

BOOK LISTS AND CATALOGUES SENT FREE ON REQUEST

BRITISH MADE THROUGHOUT

REGISTERED BB TRADE MARK

Telephone
CLErkenwell 2908
Telegraphic Address
"Gasthermo, Smith, London"

The mark of precision and efficiency

If you use heat—it pays to measure it accurately

B. BLACK & SON, LTD.

180 Goswell Road, London, E.C.1

Thermometer Manufacturers (Mercury in Glass Type)
Original Makers of the Improved, Gas filled, Permanent Thermometers for Laboratory and Industrial Processes
Standard Thermometers of the highest accuracy covering over a range from minus 200 to plus 520° C.
The National Physical Laboratory Certificates supplied with any type if required
Of all the principal Scientific Instrument and Laboratory Apparatus Manufacturers

PRINTED IN GREAT BRITAIN BY UNWIN BROTHERS LIMITED, WOKING AND LONDON